DESIGN OF A PORTABLE AND COMPACT GYROSCOPIC DEVICE FOR HAND

REHABILITATION

A Thesis

by

NAMITA ANIL KUMAR

Submitted to the Office of Graduate and Professional Studies of
Texas A&M University
in partial fulfillment of the requirements for the degree of

MASTER OF SCIENCE

Chair of Committee,   Pilwon Hur
Committee Members,   Won-Jong Kim
                                   Michael Moreno
Head of Department,   Andreas A. Polycarpou

August 2017

Major Subject: Mechanical Engineering

ABSTRACT

User centered design is an apt process for developing assistive devices, as user needs are given the utmost importance in this approach. On studying current, state of the art hand rehabilitation devices, it was inferred that there exists a need for a compact and portable hand rehabilitation device – one suitable for patients with adversely limited active range of motion of the hand. This thesis proposes a novel hand-held, portable device that is composed of a fully actuated rotor-gimbal assembly (US Patent Application: 62/413,130). The simultaneous motion of the rotor and gimbal results in a controlled gyroscopic torque that acts on the user's hand. Based on the hand's strength and mobility, the user may either synchronize the hand movement with that compelled by the device or restrict it. While the former results in the relaxation of muscles, the latter can potentially increase muscle co-ordination and muscle strength. The target specifications of the device were determined through interviews with personnel specialized in the field of hand rehabilitation. A working principle of the device was then established via a proof-of-concept model and mathematical simulations, which were further used to firm up the design parameters. The dynamic analysis of the device was then conducted to attest the structural integrity. Also, the range of forces imposed by the device on the hand were evaluated to be within safe measures through simulation and consecutive comparison with existing literature. Future work includes fabricating the final device and evaluating its performance via experiments with human subjects.

DEDICATION

This thesis is dedicated to my family. For it is their undying support and encouragement that has allowed me to bloom and grow. Such is the kind of support I wish to provide to all students who dream of changing the world for the better.

ACKNOWLEDGMENTS

CONTRIBUTORS AND FUNDING SOURCES

NOMENCLATURE

HRD	Hand Rehabilitation Device
O	Center of gravity of object being gripped
C_i	Point of contact
f_z	Normal force at point of contact
f_x	Shear force at point of contact along x axis
f_y	Shear force at point of contact along y axis
μ	Static friction coefficient
τ_y	Torque about normal at point of contact
γ	Torsional friction coefficient
DC	Direct current
3D	Three Dimensional
PI	Proportional Integral
IMU	Internal Measurement Unit
I^2C	Inter-integrated Circuit
q	State vector
DH	Denavit Hartenberg
T_i	Transformation between co-ordinates i and $i-1$
m_i	Mass of component i
I_i	Inertia of component i
K_i	Kinetic energy of component i
v_i	Linear velocity of component i

ω_i	Angular velocity of component i
R_i	Rotation between co-ordinate i with respect to global co-ordinate
P_i	Potential energy of component i
g	Gravity vector
r_{C_i}	Position vector of the center of mass of component i with respect to joint i
J_i	Jacobian corresponding to component i
L	Lagrangian
τ	Torque input
M	Mass matrix
C	Coriolis and centrifugal matrix
G	Gravitational matrix
u	Control input
h	Constraints
J	Jacobian for constrained dynamics
f	Constraining force
PM	Permanent magnet
ISO	International Organization for Standardization
PLA	Polylactic acid
FOS	Factor of Safety
CAD	Computer Aided Design
p_{OC_i}	Position vector between center O and contact point C_i
R_{OC_i}	Rotation matrix center O and contact point C_i
B_{C_i}	Wrench basis

F_{C_i}	Wrench at contact point C_i
U	Unitary matrix
V	Unitary matrix
S	Matrix with singular values

TABLE OF CONTENTS

Page

LIST OF FIGURES

LIST OF TABLES

1. BACKGROUND AND INTRODUCTION

From simple daily activities to intricate dexterous movements, the hand plays an essential role in our lives. Injuries and diseases, or disorders such as strokes, osteoarthritis, Carpal Tunnel Syndrome limit the functionality of this vital extremity [11]. About 795,000 people suffer from stroke in the United States every year [12], making it a leading cause of disability in the United States [13]. Studies aimed at measuring the functionality of the hand post-stroke recorded poor grip strength [14, 15, 9] and a reduced ability to perform daily activities such as buttoning shirts and cutting vegetables [16]. Stroke patients are also troubled by hand spasticity that is onset by contracted hand muscles [17]. Additionally, hand muscle contractions force the hand to assume a constant flexed state (closed position), which is difficult to deviate from owing to the stiffness.

Furthermore, other causes of hand disabilities such as osteoarthritis and Carpal Tunnel Syndrome affect a large segment of the population. Over 30 million US adults have been diagnosed with osteoarthritis in 2017 [18]. Further, with 463,637 annual occurrences, carpal tunnel release surgery is among the most common surgeries of the hand and wrist [19]. Studies have also shown that aging limits the active range of motion of the wrist [20]. Most patients undergo physical therapy [21] to combat these symptoms.

A popular form of therapy is occupational therapy. Here, patients perform exercises that resemble daily activities such as cutting vegetables, eating, and gripping objects of different shapes [22]. Although these procedures have proven beneficial in improving hand functionality, they suffer from a major limitation – patients must report to a therapy or rehabilitation center on a regular basis.

1.1 State of the art hand rehabilitation devices

With the deliver-on-demand services gaining popularity in several markets, it is not a surprise that patients undergoing rehabilitation also wish for such flexibility in therapeutic services [23]. Many companies have attempted to satisfy this need by developing in-home rehabilitation devices. This section details currently available products both in the market and in academia.

The Saeboglove is a glove like device that helps users combat the previously mentioned muscle contractions [1]. It is composed of tensioned strings that stretch along the dorsal side (back) of each finger. These tensioned lines perform a function like that of finger extensor muscles; they help extend fingers and consequently open the hand. With the aid of this device, users can easily open their hand and grab objects.

Another wearable rehabilitation device is MusicGlove, which focuses on finger pinching and hand coordination [2]. This system exploits the ability of rhythm or music based therapy to accelerate rehabilitation. It consists of a glove with sensors mounted on the finger tips that sense individual finger pinches. The user is asked to co-ordinate their finger pinches with a rhythmic game played on a tablet. The entertaining aspect of this process motivates the user throughout the rehabilitation process.

The Exo-glove is a portable device that helps improve in finger pinching performance [3]. The said device is a soft wearable glove lined with actuated tendons. The tension along the tendons is adjusted in accordance to the task being performed. The current system accommodates the thumb, index and the middle finger [24].

Despite the technological advancements in the field of hand rehabilitation, many patients are still forced to attend physical therapy sessions at clinics to overcome their disabilities. This thesis is aimed at the development a compact and portable rehabilitation product that would rehabilitate the hand in a holistic manner. Drawing inspiration from

the state of art devices, it is believed that the proposed device can reduce the number of therapy sessions that a patient must undergo.
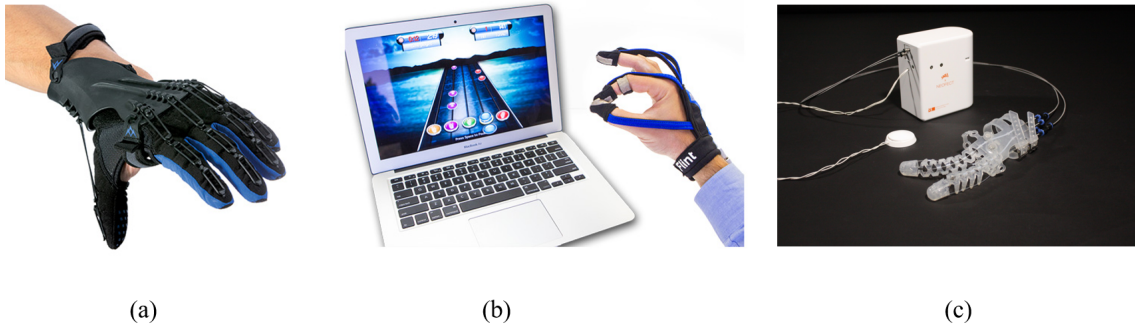
Figure 1.1: State of the art: (a) SaeboGlove [1] (b) MusicGlove [2] (c) Exo-Glove [3]

1.2   Application of the gyroscopic effect as a rehabilitation tool

It has been stated that future hand rehabilitation devices must be easy to operate, suitable for in-home rehabilitation, and economical [23]. One important example is the GyroGlove by Imperial College, London [4]. This glove can stabilize hand tremors using the torque developed by a built-in gyroscope.

Figure 1.2: GyroGlove [4]

3

Next, the NSD Powerball is a commercially available compact hand exercise product that works on the gyroscopic principle. Shaped almost like a ball, it consists of a rotor-gimbal assembly that precesses when the user applies a torque about the wrist [5]. This gyroscopic effect builds up so long as the hand motion remains synchronous with the precession. Thus, a synchronized hand motion accelerates the rotor and consequently increases the reaction forces acting on the user's muscles [25]. This continuous excitation of the hand muscles leads to improved strength and coordination. Given the nature of this device, it requires a well-functioning range of motion to operate it. Hence, it is a favored exercise tool for athletes. It also serves as a rehab tool for those suffering from arthritis, Carpal Tunnel Syndrome, and those recovering from injuries or surgeries. But, it is not suitable for patients suffering from severe hand disabilities that adversely limit the wrist's active range of motion. Nonetheless, its working principle serves as an inspiration to the product proposed in this thesis.

Figure 1.3: NSD Powerball ®[5]

Analogous to the mechanism of the Powerball ®, it is possible to create a handheld device which, upon providing the spin and precession of the rotor as inputs, produces an output gyroscopic torque. This torque would be imposed on the hand holding the device, and will consequently force the hand to move about the wrist. Researchers at

4

University of Minho attempted to accomplish this objective by actuating the rotor in the NSD Powerball ®[26]. However, the device was under-actuated and still required a user input to generate a gyroscopic effect. Hence, its customer reach would be limited to those with a functioning active range of motion.

This thesis proposes a new Hand Rehabilitation Device (HRD) that consists of a fully actuated rotor-gimbal assembly. Unlike the aforementioned products, the torque developed by the HRD does not demand user input. It is strongly believed that the HRD would be accessible to all patients troubled by hand disabilities, regardless of the extent of disability.

1.3   Development of a generic market-pull product

Once an opportunity for a new product has been identified, a process-centric approach that caters towards the identified market need, can be adopted. Fig. 1.4 depicts a generic product design process used for market-pull products. This approach commences by identifying customer needs and concludes with the final product [6]. The designer is also required to simultaneously conduct a cost analysis, competitive benchmarking (which is to study the state of the art), and build test models and prototypes.
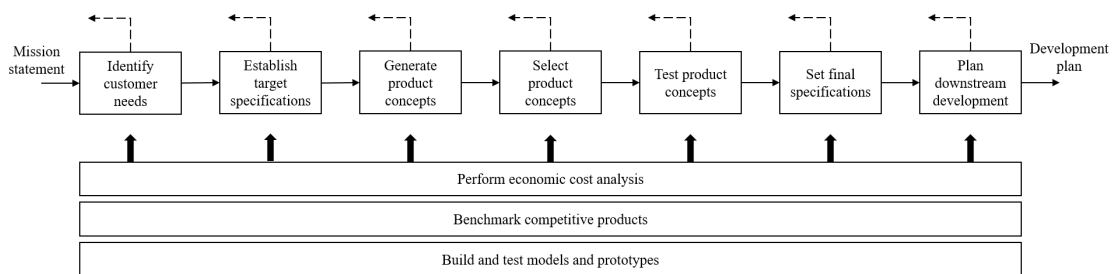
Figure 1.4: Generic product design process [6]

A common issue experienced during the design of innovative products is conflicting design requirements. For instance, it may be desired that a product must have high inertia while low weight. A favorable method of resolving such issues is to implement TRIZ (A Russian terminology, roughly translated as the theory of resolving invention-related tasks) design principles [27]. TRIZ is composed of 40 design principles that can be implemented towards developing innovative concept designs that satisfy all target specifications.

1.4   Voice of customer

The primary customers of a new rehabilitation device would be the patients with hand disabilities. But it should be duly noted that most patients ask for their therapist's/doctor's recommendations prior to investing in a rehabilitation tool. Hence physical and occupational therapists were interviewed to develop an understanding of what is expected from a hand rehabilitation device.

Dr. Binal Motawar, a physical therapist from PeaceHealth St. John Medical Center in Washington State, was interviewed to shed light on the current therapeutic practices and commercially available hand rehabilitation devices. The interview also generated information about the needs that the proposed device should satisfy. It was gathered that a device that imposes a torque on the hand would definitely aid in rehabilitation. There are two kinds of therapies that can be implemented with such a device: one involving synchronizing with the torque and another requiring the user to resist the torque. Each method targets different hand disabilities. Firstly, spasticity, which is caused by contracted muscles, can be countered by passively moving joints through the range of motion [28]. The imposed torque compels the user's hand to move about the wrist. So long as the user does not counter the torque, but remain synchronous with it, the hand muscles will continue to relax. Secondly, users with some active range of motion conduct exercises to improve their grip force and wrist strength. Such improvements can potentially be acquired while

6

using the proposed device by countering the torque imposed and arresting the hand. In order to do so, users will have to constantly re-position their wrist according to the torque's direction. Further, to maintain grip, users will have to manipulate the pressure imposed by their fingers according to the change in torque. Such actions improve muscle coordination and potentially aid in increasing strength [29].

Ms. Angela Brown, a physical therapist at Generations Center for Senior Living, stated that several senior citizens often fail to attend all therapy sessions. Thus, she believed an in-home rehabilitation that can be used without a therapist's supervision would be useful. It was also her opinion that electrical stimulation should be avoided since: (i) there are concerns of it causing side-effects such as high blood pressure in senior patients and (ii) it may delay FDA approval. She reflected that many of the current rehabilitation devices are either too expensive or bulky and that patients could easily accept an economic and compact device.

Dr. Xiao Lee, M.D. in Affiliated Hospital of Nanjing University of TCM, also expressed that several stroke patients, especially those who have limited range of motion, tend to depend on others to drive them to the rehabilitation centers. Thus, such patients would prefer an in-home rehabilitation device. Moreover, patients would be attracted towards easy to operate devices. Adding to the previous argument, stroke patients often find themselves unable to carry heavy objects and grasp them properly in their hands. Dr. Lee stressed the need for rehabilitation devices to be lightweight to facilitate a more comfortable hand rehabilitation regime.

1.5 Fabrication of custom designed components

The proposed product is required to house two actuators (one that controls the rotor and another for the gimbal) while being compact and lightweight. These requirements demand an innovative design that would feature components with custom and complex geometries.

Standard manufacturing processes like injection casting would raise the expenses on the product development process. Hence, alternate measures of fabrication must be pursued [30].

Additive manufacturing, at times referred to as 3D printing, has been gaining popularity in the field of custom manufacturing. It has transitioned from being a rapid prototyping process to a main stream fabrication technique. Among the unique characteristics it has to offer, its ability to produce lightweight and complex components cannot be overlooked. The weight of a component can be adjusted by controlling the print density and by wisely choosing the print material [31]. The surface finish of the printed part strongly depends on the printer's resolution [31].

Powder bed fusion process is a form of additive manufacturing that uses a laser to sinter powder (fine particles of the print material) to a desired form. It operates in a layer based manner where every layer corresponds to a cross section of the final product. Once the laser sinters a layer, a roller deposits a fresh film of powder and the process continues [31, 7]. Fig. 1.5 is a schematic of powder bed fusion process.
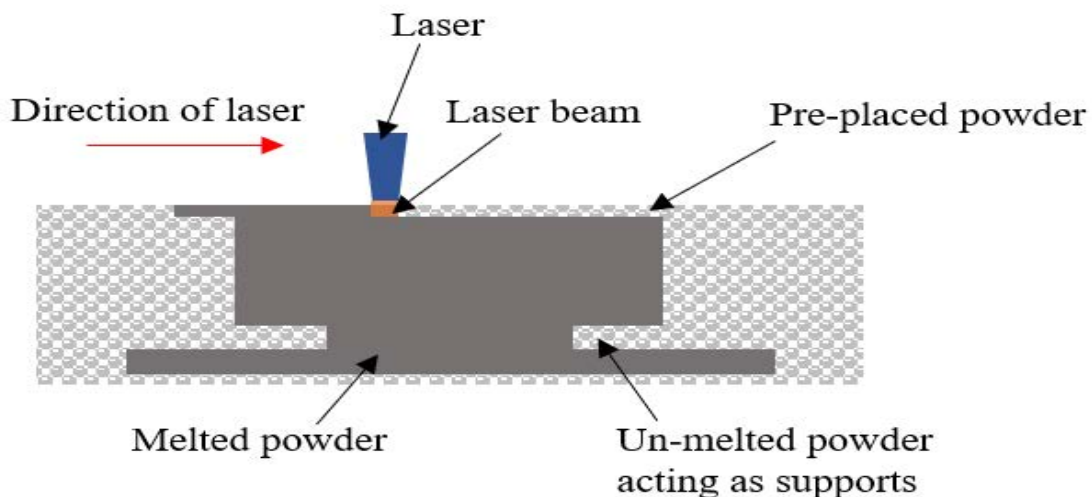
Figure 1.5: Schematic of powder bed fusion process [7]

The part density of powder bed fusion process depends on the size of the particles used and the radius of laser beam [31, 7]. By choosing a smaller laser beam size and finer powder, one can produce high resolution parts with a smooth surface finish [31, 7]. Another major benefit of this technique is that the printing process does not require any additional support structures for overhanging elements. This is so because the underlying non-sintered powder inherently forms the support for the overhanging structures [31, 7].

1.6   Understanding grip and the associated forces acting on the hand

An important factor that must be considered while designing hand rehabilitation devices is the range and distribution of forces imposed on the hand by the device. Care must be taken to ensure that the resulting forces do not induce slipping at the contact point. Further, the imposed forces should not exceed the range of forces that can be safely tolerated by the user.

The initial step in studying the imposed forces would be to model the contact between the human hand and the object. Given an object with a Center of Gravity (CG) O, a force will be imposed at the point of contact C_i. This setup has been shown in Fig. 1.6.

Forces and torques, both, could be imposed at the point of contact. A vector composed of forces and torques is termed a wrench. The type of contact can be categorized as follows.

i) Frictionless point contact - Involves only a normal force f_z at C_i. This type of contact has been depicted in Fig. 1.6. Note that $f_z \geq 0$.

ii) Columb friction model - Involves a normal force f_z and shear forces f_x and f_y such that $\sqrt{f_x^2 + f_y^2} \leq \mu f_z$, where μ is the coefficient of friction. Refer Fig. 1.6 for more details.

iii) Soft contact - Involves a normal force f_z and shear forces f_x and f_y, as in case of the

9
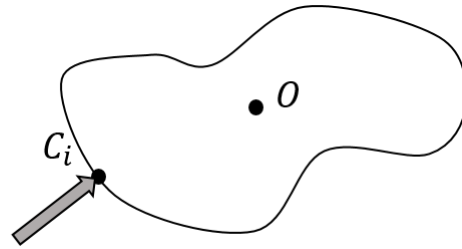
(a) Object center – O and contact point – C_i
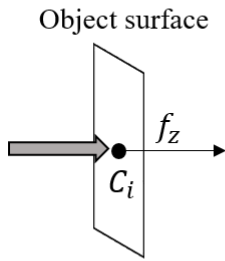
(b) Frictionless point contact
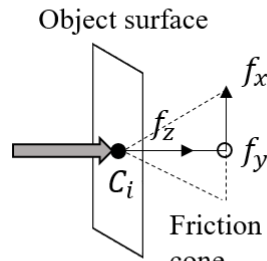
(c) Columb Friction model
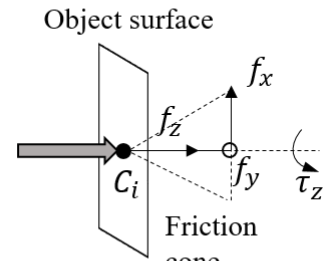
(d) Soft contact

Figure 1.6: Modeling contact between an object with center O and a contact point C_i. Figures (b), (c), and (d) depict different contact models [8]

Columb Friction model. Additionally, a torque τ_z acts about the normal direction such that $|\tau_z| \leq \gamma f_z$ where γ is the torsional coefficient of friction. Fig. 1.6 depicts the orientation of these forces.

It is also noted that all forces discussed in the latter two models can be perceived to act within a cone referred to as the friction cone. This is due to the nature of their magnitudes and directions.

Several studies are directed towards achieving and analyzing the forces that are imposed by a hand during static grip. A common procedure to evaluate such forces is to use a cylindrical dynamometer [32, 9]. Both [32] and [9] model the contact as per the Columb friction model. While [32] studied the contact forces experienced by healthy adults, [9]

10

dealt with stroke patients. Both studies concluded that during a power grip (when the subject imposes maximum force), the distal phalanx imposes the maximum force compared to the middle and proximal phalanx. It has been reported in [9], that the maximum force stroke survivors can impose is $154N$ while healthy adults can impose $270N$. Fig. 1.7 shows the percentage contribution of each finger towards the total normal force, as per [9]. An interesting note was that the percentage contributions recorded for both healthy and stroke survivors were approximately the same. Note that Digit I in Fig. 1.7 corresponds to the thumb, while Digit V represents the little finger.
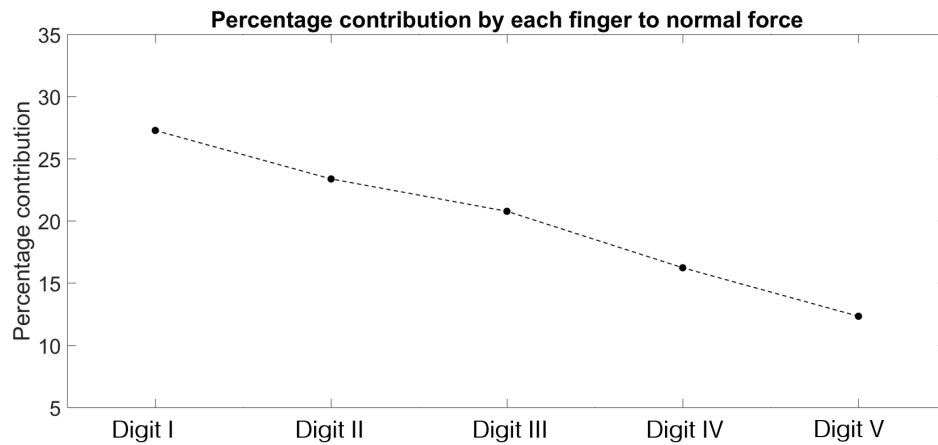
Figure 1.7: Contribution of each finger to the total normal force [9]

2.   CONCEPT DESIGN*

To ensure that all objectives are met within the given time frame, a process-centric design approach was adopted [6]. The mission statement of this product development process was to create a portable and compact hand rehabilitation device for all users that experience hand disabilities. The study of current hand rehabilitation devices and the data collected through interviews with therapists served as the competitive benchmarking and customer needs data, respectively. The target specifications were based on the data collected. Some of the information provided in the following sections have been presented at the South Central American Society of Biomechanics Conference, 2017.

2.1   Target Specifications

Occupational therapy is a common therapeutic practice implemented to combat hand disabilities [33]. It requires patients to carry out routine activities such as cutting vegetables, eating and gripping objects of varying shapes. Studies have shown that a wrist torque of 0.7 Nm is required for opening a jar's lid (an activity practiced during occupational therapy) [34]. It was thus decided that the HRD should be capable of producing a gyroscopic torque of 0.7 Nm.

Further, assistive devices that are entertaining and aesthetically pleasing are known to produce faster and better results compared to those that are not; emphasizing the need for the HRD to have a good user appeal [35]. With regard to the shape, a ball shaped device was preferred since a ball is a commonly used tool in occupational therapy. The weight of the device had to be carefully considered in order to minimize the strain on the user's hand. The mass of a commonly carried half-a-liter water bottle (approximately 550 g)

Table 2.1: Target specifications

Feature	Specification
Weight	Less than 550 g
Portable	All electronics and mechanical components must be made portable
Size	Within sphere of diameter 80 mm
Torque output	Output gyroscopic torque of 0.7 Nm
Shape	A spherical shape is preferred

was selected as the ideal target for the device's mass. Portability was yet another desired feature so that users could undergo rehabilitation anywhere and anytime. The desired product specifications have been summarized in Tab. 2.1.

As stated earlier, the HRD would target all those who have hand disabilities. Given the nature of the proposed device, especially with the desire to mimic the shape of a ball, the ability to grip the device might be a prerequisite to operating it. Thus, it might not bode well with patients who lack grip strength. The final design must meet all target specifications while duly accounting for the possibility of low grip strength. The specifications need not be satisfied by the device alone; accessories for the device can be designed to accomplish certain target specifications.

2.2 Principle

The device consists of an actuated rotor and gimbal, which upon actuation, produce a gyroscopic torque that is imposed on the user's hand. Consider Fig. 2.1 where the red, blue and green components represent the user's hand, gimbal, and the rotor, respectively. While the motion about the rotor's axis is referred to as spin, the movement about the gimbal's axis is called precession. The result of spin and precession is a gyroscopic torque that predominantly acts about a direction mutually perpendicular to the rotor's and gimbal's

axes [36].
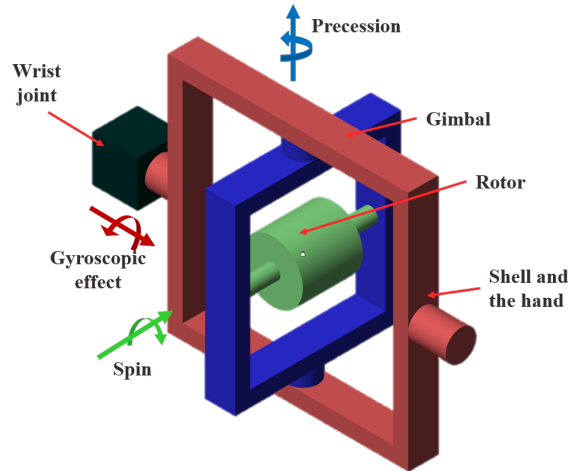
Figure 2.1: Device schematic

2.3   Proof of concept

To understand the working principle, a proof of concept model was constructed as shown in Fig. 2.2. The model consisted of a fully actuated rotor-gimbal assembly and a bracket that was held by a subject. An experiment was then conducted to investigate how the hand motion, compelled by the device, varies with the motion of the rotor and gimbal.

2.3.1   Mechanical and Electrical configuration

Fig. 2.2 depicts all the mechanical components used. The assembly consisted of two motors: (i) Motor-1 was a brushless 50 Watt DC motor (Maxon EC-*i* with 40 mm housing diameter) and was operated using a Maxon 24×2 DEC motor driver, and (ii) Motor-2 was a brushed DC motor Pololu 12 V, 29:1 Gear Motor with an encoder and was operated through a Sabertooth 2×5 motor driver. Motor-1 was affixed to a 3D printed bracket using

a clamp. The said bracket was then secured to the shaft of Motor-2 via a set screw hub. Motor-2, on the other hand was attached to a bracket held by the user's hand.
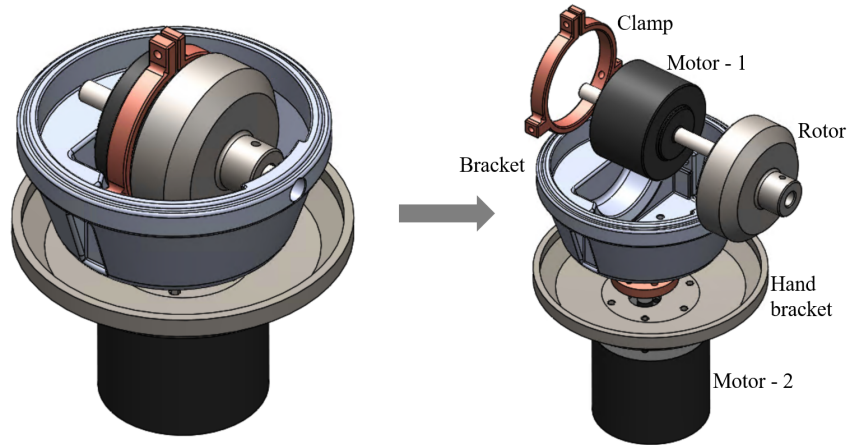
Figure 2.2: Proof of concept with both rotor and gimbal actuated

A NI MyRio was used to control the motion of both motors. To avoid entanglement of wires, the gimbal's movement was limited to a to and fro motion about its axis. A PI controller, with the proportional gain $= 1.03$ and integral gain $= 1.15$ (both manually tuned), was used to control and monitor the speed of the gimbal. Fig. 2.3 shows the actual gimbal speed versus the desired gimbal speed on implementing the PI controller. The desired gimbal speed was given by $6.28 \sin(2t)$ rad/s. No speed controller was implemented for the rotor since the DEC 24×2 inherently implements a PI controller.

An Internal measurement unit (IMU) was positioned on the dorsal side of the ring and little finger, to measure the motion of the hand. The selected IMU was the MPU 9150. An Arduino Uno was used to gather raw data from the IMU using the I^2C library by Jeff Rowberg [37]. A complementary filter was then implemented to process the measured

pitch and roll angles. While the pitch corresponded to flexion and extension of the hand, the roll represented supination and pronation.
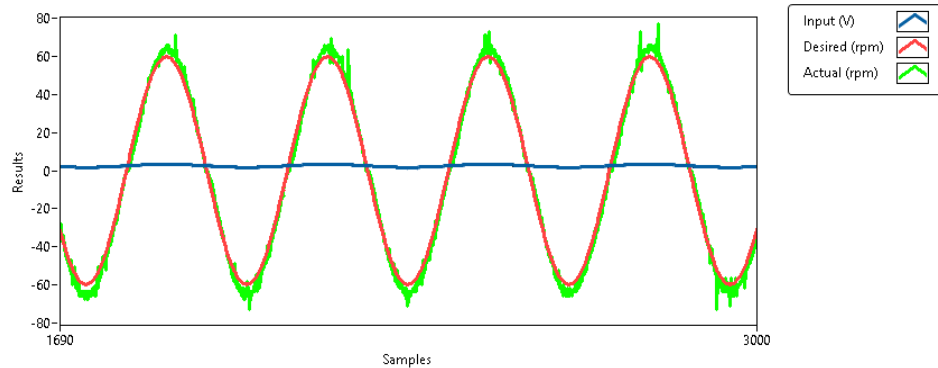
Figure 2.3: Results of implementing PI controller for the gimbal

2.3.2   Proof of Concept experiment

The experimental set up has been shown in Fig. 2.4. A total of 7 tests were carried out with one subject. Each test lasted a minute during which both the rotor and gimbal were actuated. 3 key parameters could be varied in the experimental setup:

i) The amplitude of gimbal speed

ii) The period of oscillation of the gimbal

iii) The speed of the rotor

Pilot runs were conducted in order to develop an understanding of the system and its affect on the subject's hand. Based on the data from the IMU, an initial understanding of the system was derived. The 7 tests were then conducted in accordance to the observations during the pilot runs.

16
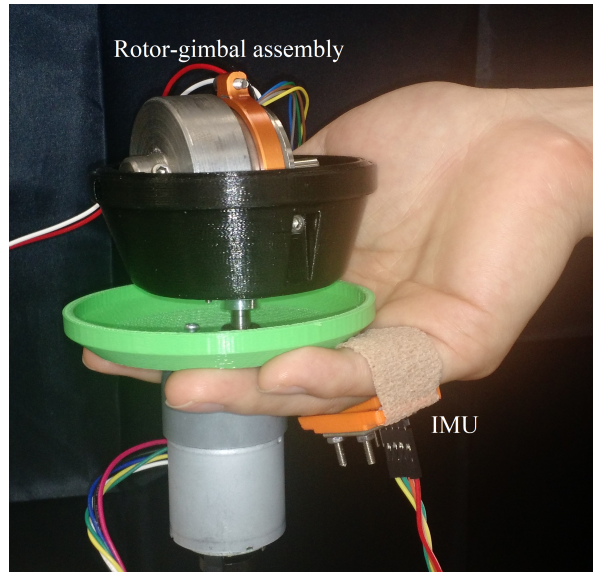
Figure 2.4: Proof of concept - experimental setup

The tests conducted have been enumerated in Tab. 2.2. Test 0 was considered as the baseline. Details of the Proof of Concept model such as those of the electrical system, the Labview program, and the Arduino code have been provided in Sec. B.1.

Table 2.2: Tests conducted during Proof of Concept

Set	Test No.	Gimbal speed (rad/s)	Rotor speed (rad/s)
Baseline	0	$6.28\sin(2t)$	230.38
Varying speed magnitude of gimbal	1.1	$4.19\sin(2t)$	230.38
	1.2	$8.38\sin(2t)$	230.38
Varying gimbal's frequency of oscillation	2.1	$6.28\sin(1.5t)$	230.38
	2.2	$6.28\sin(2.5t)$	230.38
Varying rotor's speed	3.1	$6.28\sin(2t)$	136.14
	3.2	$6.28\sin(2t)$	324.63

17

2.4 Modeling and Simulation

The mathematical model consists of 5 degrees of freedom – three describe the motion of the wrist [38] while the remaining correspond to the motion of the gyroscope's rotor and gimbal. The degrees of freedom have been enumerated as follows:

i) Wrist pitch q_1 - flexion & extension

ii) Wrist yaw q_2- radial & ulnar deviation

iii) Wrist roll q_3- pronation & supination

iv) The precession of the rotor and-gimbal assembly q_4

v) Rotor spin q_5

Hence the state vector is given by:

$$q = \left\{ q_1 \quad q_2 \quad q_3 \quad q_4 \quad q_5 \right\}^T \tag{2.1}$$

2.4.1 Model schematic

The co-ordinates for the modeled system have been depicted in Fig. 2.5. It was assumed that the design of the gimbal and rotor would be such that their co-ordinate origins are coincident. This assumption was later considered as a design requirement since it minimizes any rotary imbalances that could result in vibrations and consequently cause discomfort to the user. Further, for the sake of simplicity, it was also assumed that this common origin would be aligned with the wrist's origin as shown in Fig. 2.5.

2.4.2 Equations of motion

The governing equations of motion for the system can be derived via Euler-Lagrange equations. Using Denavit Hartenberg (DH) conventions [39], a DH table relating the co-
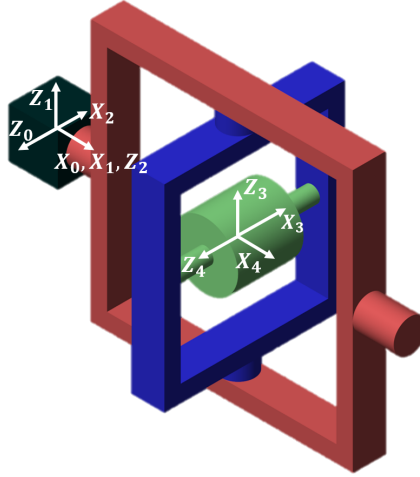
Figure 2.5: Joint co-ordinates

ordinates of each degree of freedom was constructed. The DH table for the system is shown in Tab. 2.3. The orientation and position of co-ordinate i with respect to $i-1$ co-ordinate axis is given by the following transformation.

$$
T_i = \begin{bmatrix} cos(q_i) & -sin(q_i) & 0 & 0 \\ sin(q_i) & cos(q_i) & 0 & 0 \\ 0 & 0 & 1 & 0 \\ 0 & 0 & 0 & 1 \end{bmatrix} \begin{bmatrix} 0 & 0 & 0 & 0 \\ 0 & 0 & 0 & 0 \\ 0 & 0 & 0 & d_i \\ 0 & 0 & 0 & 1 \end{bmatrix} \begin{bmatrix} 0 & 0 & 0 & a_i \\ 0 & 0 & 0 & 0 \\ 0 & 0 & 0 & 0 \\ 0 & 0 & 0 & 1 \end{bmatrix} \begin{bmatrix} 1 & 0 & 0 & 0 \\ 0 & cos(q_i) & -sin(q_i) & 0 \\ 0 & sin(q_i) & cos(q_i) & 0 \\ 0 & 0 & 0 & 1 \end{bmatrix}
$$

$$(2.2)$$

If the mass and inertia of component i are m_i and I_i, respectively, then its kinetic (K_i) and potential (P_i) energy are given by:

$$
K_i = \frac{1}{2}m_i v_i^T v_i + \frac{1}{2}\omega_i^T R_i I_i R_i^T \omega_i,
$$

$$(2.3)$$

Table 2.3: DH Table with angles in radians and distances in meters

Joint	Axis	θ	d	a	α
1	Z_0	q_1^*	0	0	$-\frac{\pi}{2}$
2	Z_1	$q_2^* + \frac{\pi}{2}$	0	0	$\frac{\pi}{2}$
3	Z_2	q_3^*	0.055	0	$-\frac{\pi}{2}$
4	Z_3	$q_4^* - \frac{\pi}{2}$	0	0	$\frac{\pi}{2}$
5	Z_4	q_5^*	0	0	0

$$P_i = g^T r_{C_i} m_i, \tag{2.4}$$

where v_i and ω_i are the linear and angular velocity of the center of mass of component i with respect to the global co-ordinate system. R_i is the rotation matrix with respect to the co-ordinate axes. The vector g represents the gravitational component, while r_{C_i} is the position vector of the component's center of mass with respect to joint i. Furthermore, the linear and angular velocities of the component are given by the Jacobian J_i and the derivative of the state vector q.

$$\begin{Bmatrix} v_i \\ \omega_i \end{Bmatrix} = \begin{Bmatrix} J_{v_i}(q) \\ J_{\omega_i}(q) \end{Bmatrix} \dot{q}, \tag{2.5}$$

Since the first three co-ordinates represent the motion of the same component, the mass and inertia corresponding to the component are associated only with the final co-ordinate of the sequence, that is q_3. There are essentially only three components in the system of which the energy is evaluated. Hence, the total kinetic energy (K) and potential energy (P) have provided in the following.

$$K = \frac{1}{2}\dot{q}^T \sum_{i=3}^{5}(m_i J_{v_i}^T J_{v_i} + J_{\omega_i}^T R_i I_i R_i^T J_{\omega_i})\dot{q} = \frac{1}{2}\dot{q}^T D \dot{q} \tag{2.6}$$

$$P = \sum_{i=3}^{5} g^T r_{C_i} m_i, \tag{2.7}$$

Matrix D is called the inertia matrix of the system. Further, the Lagrangian L and the corresponding equation of motion has been derived.

$$L = \frac{1}{2}\dot{q}^T D\dot{q} - P$$

$$\implies \frac{d}{dt}\frac{\partial L}{\partial \dot{q}} - \frac{\partial L}{\partial q} = \tau$$

$$\implies \sum_{i=1} m_{kj}(q)\ddot{q}_j + \sum_{i,j} c_{ikj}(q)\dot{q}_i\dot{q}_j + g_k(q) = \tau_k \ \ for \ \ k = 1, 2...5,$$

$$\implies M(q)\ddot{q} + C(\dot{q},q)\dot{q} + G(q) = \tau, \tag{2.8}$$

where $M(q)$ is the inertial matrix, $C(\dot{q},q)$ is the Coriolis/centrifugal matrix, and $G(q)$ is the gravity vector. These matrices were validated using the Robotica package in Wolfram Mathematica [40]. Finally τ was the input torque to the system. Eqn. 2.8 can be extended to include a control input u as shown in Eqn. 2.9.

$$\implies M(q)\ddot{q} + C(\dot{q},q)\dot{q} + G(q) = Bu + \tau, \tag{2.9}$$

2.4.3 Constrained dynamics

To acquire the torque acting at the wrist, all three degrees of freedom of the wrist were arrested; that is $q_1 = q_2 = q_3 = 0$. The resulting dynamics was termed constrained [8]. The term $h(q)$ represents the constraints imposed.

$$h = \left\{ q_1 \quad q_2 \quad q_3 \right\}^T = \vec{0}$$

$$\Longrightarrow h = \begin{bmatrix} 1 & 0 & 0 & 0 & 0 \\ 0 & 1 & 0 & 0 & 0 \\ 0 & 0 & 1 & 0 & 0 \end{bmatrix} q = \vec{0}$$

$$\Longrightarrow \frac{dh}{dt} = \frac{dh}{dq}\frac{dq}{dt} = \vec{0}$$

$$\Longrightarrow J\dot{q} = \vec{0}$$

$$\Longrightarrow J\ddot{q} + \dot{J}\dot{q} = 0 \tag{2.10}$$

Now, the constraining force was derived by substituting $\ddot{q}$ using Eqn. 2.9. Note that the torque τ was represented in terms of the constraining force f. To elaborate, $\tau = J^T f$.

$$\Longrightarrow J(-M^{-1}C\dot{q} - M^{-1}G + M^{-1}Bu + M^{-1}J^T f) + \dot{J}\dot{q} = 0$$

$$\Longrightarrow JM^{-1}J^T f = JM^{-1}C\dot{q} + JM^{-1}G - JM^{-1}Bu - \dot{J}\dot{q}$$

$$\Longrightarrow f = (JM^{-1}J^T)^{-1}(JM^{-1}(C\dot{q} + G - Bu) - \dot{J}\dot{q}) \tag{2.11}$$

The equations of motion for the constrained system were then determined by evaluating Eqn. 2.9, given the newly acquired constraining force. For the given constraints, the derivative of the Jacobian with respect to time, namely $\dot{J}$, is equal to 0.

$$\Longrightarrow M\ddot{q} = -C\dot{q} - G + Bu + J^T(JM^{-1}J^T)^{-1}(JM^{-1}(C\dot{q} + G - Bu))$$

$$\Longrightarrow \ddot{q} = M^{-1}(J^T(JM^{-1}J^T)^{-1}JM^{-1} - I)(C\dot{q} + G) + M^{-1}(I - J^T(JM^{-1}J^T)^{-1}JM^{-1})Bu \tag{2.12}$$

Then, the equations of motion of the rotor and gimbal, for the initial conditions prescribed in Eqn. 2.13 and Eqn. 2.14, were solved in MATLAB. Details regarding the packages and code to determine and solve the equations of motion have been provided in Sec. B.2. The derived equations were also validated using a model built in Simscape, a Mathworks package. Sec. B.2 also provides images of the Simscape model.

$$q_0 = \left\{ 0 \quad 0 \quad 0 \quad 0 \quad 0 \right\}^T \tag{2.13}$$

$$\dot{q}_0 = \left\{ 0 \quad 0 \quad 0 \quad 25 \quad 300 \right\}^T \tag{2.14}$$

The input parameters to the system have been enumerated in Tab. 2.4. Approximated inertias of the hand (I_H), and initial guesses for the gimbal (I_G) and rotor (I_R) inertias have been given in Eqn. 2.15 with the units kg m^2. These were also provided as input parameters to the solver.

$$I_H = 10^{-4} \begin{bmatrix} 4.42 & 0 & 0 \\ 0 & 3.39 & 1.27 \\ 0 & 1.27 & 2.21 \end{bmatrix} \qquad I_G = 10^{-5} \begin{bmatrix} 2.11 & 0 & 0 \\ 0 & 1.78 & 0 \\ 0 & 0 & 2.24 \end{bmatrix}$$

$$I_R = 10^{-5} \begin{bmatrix} 7.83 & 0 & 0 \\ 0 & 7.83 & 0 \\ 0 & 0 & 9.11 \end{bmatrix} \tag{2.15}$$

The resulting motion has been depicted in Fig. 2.6 and Fig. 2.7. Given the motion of the rotor and gimbal, reaction torques acting about the wrist were calculated and have been shown in Fig. 2.8. The values for the rotor and gimbal inertias were tweaked until

23

Table 2.4: Input parameters

Parameter	Value	Units
Rotor speed	300	rad/s
Gimbal speed	25	rad/s
Mass of rotor	0.21	kg
Mass of rotor - gimbal assembly	0.36	kg
Approximated mass of hand	0.35	kg

torques of peak-to-peak magnitude 0.7 Nm were acquired. The inertia values resulting in the desirable torques were further used to design the components of the device.
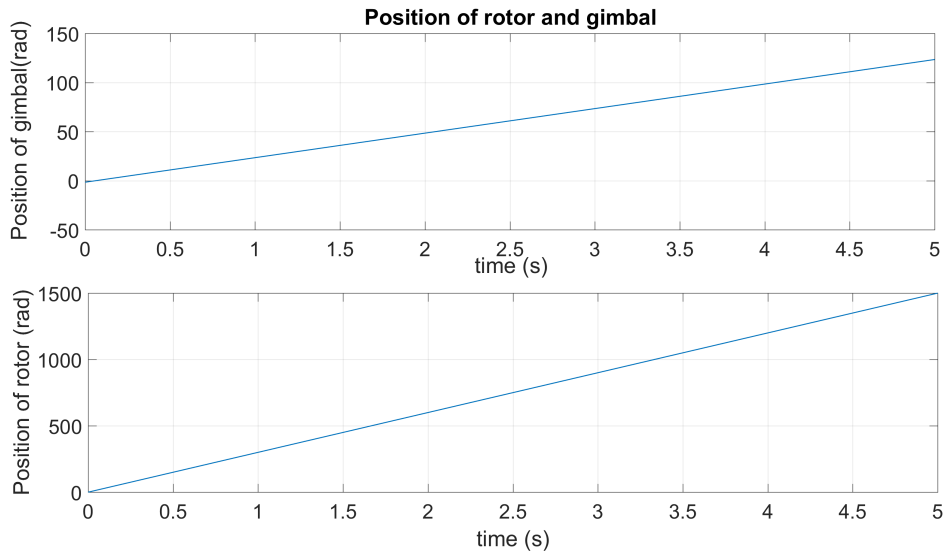
Figure 2.6: Position of the rotor and gimbal when the hand is arrested
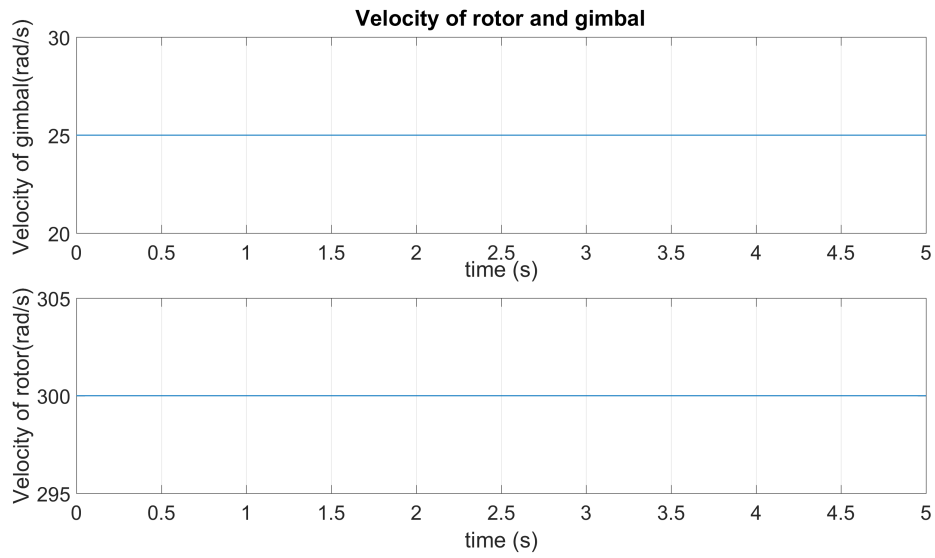
Figure 2.7: Velocity of the rotor and gimbal when the hand is arrested
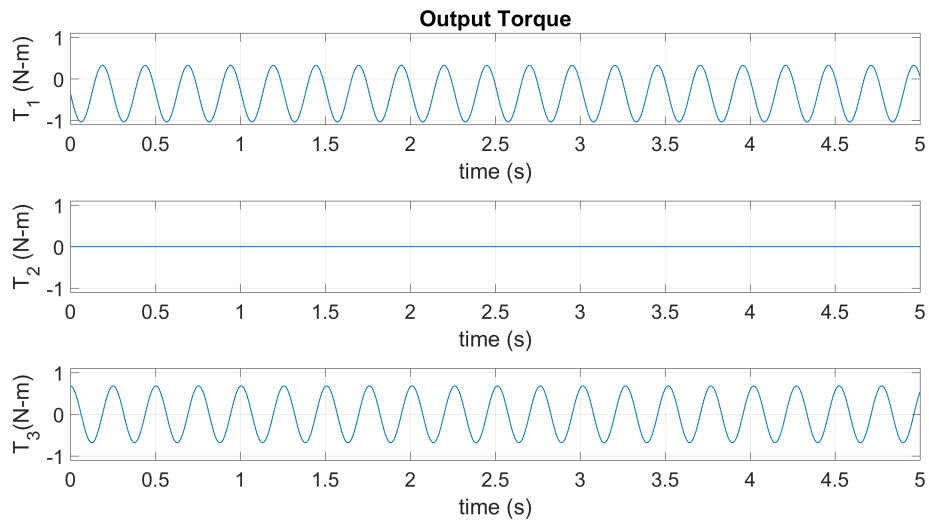
Figure 2.8: Estimated torque about the wrist when the hand is arrested

2.5 Initial concept

In accordance to requirements set by the simulation, a list of motor specifications was generated. A frame-less external rotating motor was chosen to actuate the rotor. It was understood that a custom rotor housing would have to be designed to ensure symmetry in the component. This was crucial to avoid any rotary imbalances in the system. Further, it was decided a brushless motor would be ideal to increase the longevity of the product.

The rotor assembly consisted of the motor's stator firmly affixed to the shaft. The permanent magnet rotor was then held in place by the rotor housing. It was vital that the air gap between the stator and rotor be accurate. The housing could have been designed as either a single or two-piece assembly based on the selected frame-less motor kit. But it was essential for it to be supported by suitable bearings. Apart from the aforementioned rotor assembly, the product also consisted of the gimbal, its actuation system, and the enclosure.
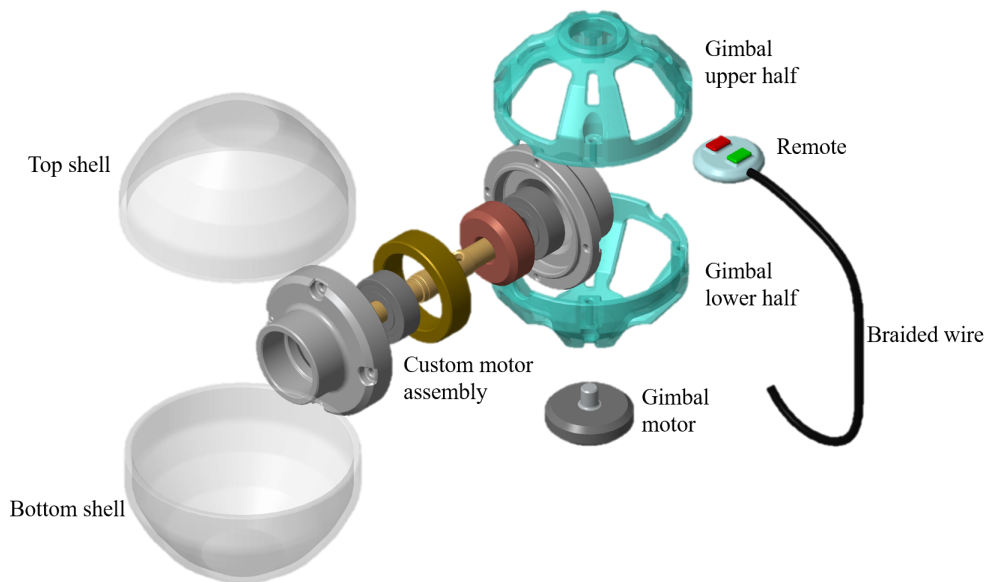
Figure 2.9: Concept design

3.   FINAL DESIGN AND ANALYSIS[*]

The greatest challenge of the design process involved minimizing the weight and size of the device. It was soon realized that the desired spherical shape could not be acquired and thus an oblong shape was adopted. The final product mimics the shape of an American football, so that it would appeal to the user and prospectively make the rehabilitation a fun process. The devices enclosure consists of a frame with snap fitted front and back covers, and end-caps. To compensate for the new shape, finger hold provisions were made on the front and back covers so that the user can hold the device along the side like they would a cup. This can be seen in the front and back view of Fig. 3.1. An exploded view of the assembly can be seen in Fig. 3.2 The dynamical impact of a side hold must be analyzed through tests, since it varies from that defined in the mathematical model.

(a)   (b)   (c)
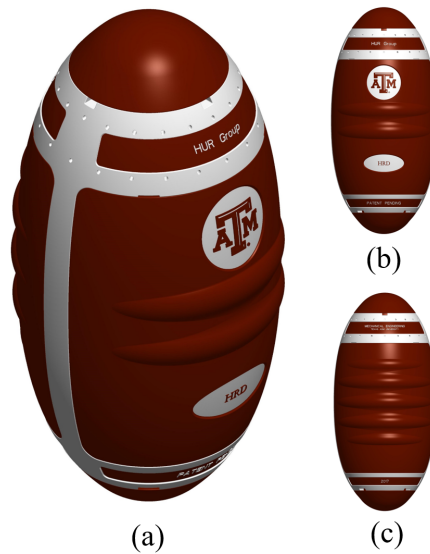
Figure 3.1: Final design: (a) Isometric view (b) Front view (c) Back view

Top end
cap

Enclosure
frame

Snap fitted
back cover

Snap fitted
front cover

Rotor – Gimbal
assembly

Bottom end cap
with hole for wires
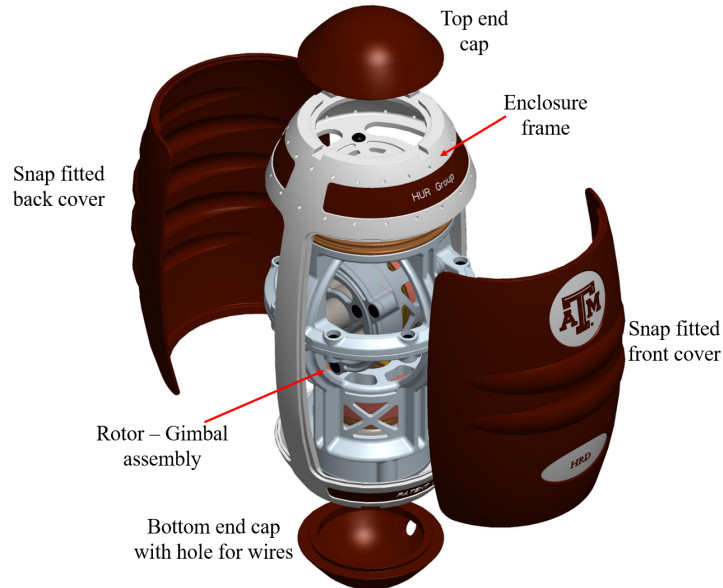
Figure 3.2: Exploded view of the enclosure frame

3.1 Mechanical Design

To make the device portable, the electronics were initially conceived to be embedded in the device. But, this idea conflicted with the need for a compact and lightweight device. Upon using TRIZ design principle - "*Taking out - Extract the disturbing part or property from an object*", both these objectives were achieved [27]. It was decided that the electrical systems would be placed external to the device in a satchel that the users can wear. While the wires to the gimbal's motor were easily drawn through a hole in the bottom end-cap, the wires for the rotor assembly were mechanically coupled to the motor's leads using a slip ring assembly. This facilitated the free precession of the rotor assembly without any entanglement of wires. The principal components of the design (namely rotor assembly, gimbal assembly, and slip ring assembly) can be seen in Fig. 3.3.
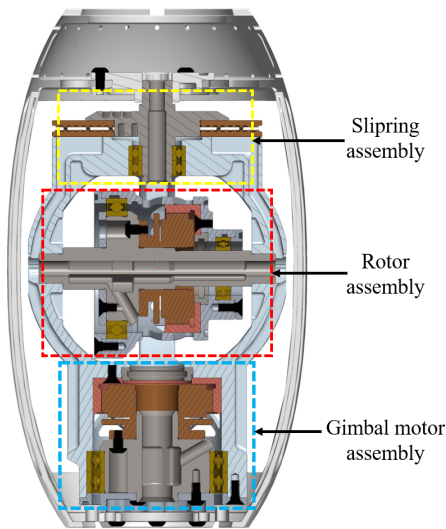
Figure 3.3: Cross sectional view of the device depicting the principal components of the assembly

Figure. 3.4 depicts the cross section of the rotor and gimbal assembly secured in the enclosure frame. The identification numbers listed in the device will be used to refer to the various components of the device. For instance, the slip ring assembly (ID #3) consists of a stationary (ID #3a) and rotating element (ID #3b). The former is secured to the enclosure frame using a flange (ID #2) and an anchoring component (ID #1).

3.1.1   Rotor – Gimbal Assembly

To ensure symmetry in the design and avoid rotary imbalances, the rotor and the gimbal housings (ID #7 and #4) were directly integrated with the permanent magnet (PM) rotor (ID #15 and #18) of the chosen brushless DC motors (Maxon EC 45 series). This design is similar to that of motorized spindles [41]. Integrating the PM rotor directly with the rotating housing facilitates high speed operations with precise control over the acceleration, while minimizing vibrations. Such a design requires enormous care while assembling

since the air gap between the PM rotor and the stator windings (ID #9 and #20) must be well maintained. To ease the process of assembling, a component termed hub locator (ID #14 and #17) was designed. This element is placed in the gimbal or rotor housing prior to the PM rotor. Its outer radial surface acts as a guide during the installation of the PM rotor and ensures that the component remains concentric with the gimbal or rotor housing and the motor shaft.

List of components with their identification number (ID #):
1. Flange Anchor
2. Flange
3. (a) Fixed component of slip ring
   (b) Rotating component of slip ring
4. (a) Upper gimbal housing
   (b) Lower gimbal housing
5. Deep groove ball bearing pair
6. Snap ring
7. Rotor housing
8. & 10. Outer bearing retainer
9. & 19. Stator coils
11. Inner bearing retainer
12. Stator shaft
13. &16. Deep grove ball bearing
14. & 17. Hub locator
15. & 18. PM rotor
19. Stator coils
20. Gimbal shaft
21. Angular contact bearings
22. Outer bearing retainer
23. Inner bearing retainer

Figure 3.4: Cross section of rotor – gimbal assembly

3.1.1.1   Gimbal Assembly Design

The gimbal housing (ID #4) consists of two halves; the lower half (ID #4b) is motorized while the upper half (ID #4a) is connected to the rotating component of the slip ring assembly (ID #3). The two halves are bolted together about the splined shaft (ID #12) of

the rotor assembly. The upper half of the assembly is supported by a pair of ISO standard deep groove ball bearings (ID #5) held in place on one side by shoulders on the flange (ID #2) and gimbal housing, and a snap ring (ID #6) on the other side. Unlike the upper half of the assembly, the lower half undergoes both radial and axial loading. Hence a pair of ISO standard angular contact bearings (ID #21) in a back-to-back arrangement, has been selected. The bearings' outer races are supported by a shoulder on the gimbal housing and inner bearing retainer (ID #23). On the other hand, the bearings' inner races are supported by a shoulder on the gimbal shaft (ID #20) and the inner bearing retainer (ID #22) as shown in Fig. 3.4. The inner and outer bearing retainers are secured to the gimbal shaft and the gimbal housing, respectively.
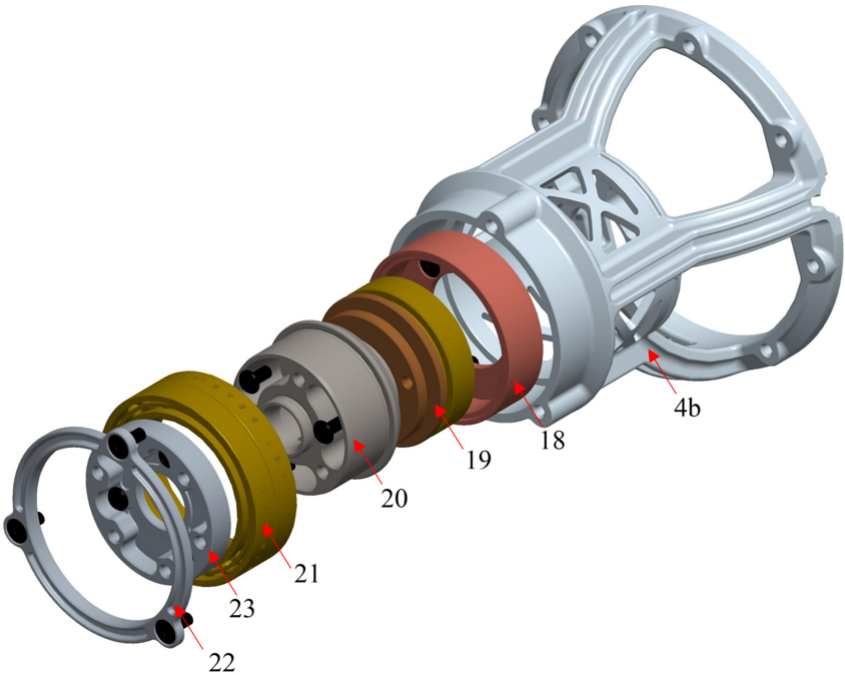
Figure 3.5: Exploded view of lower gimbal assembly

3.1.1.2 Rotor Assembly design

The rotor housing (ID #7) is a single component, the design of which greatly influences the generated torque. It was designed with a major focus on ease of assembly as it can be observed in the exploded view Fig. 3.6. It is supported by two deep groove ball bearings (ID #16 and #13) mounted on either side of the stator windings. The Bearing ID #16 is held in place by shoulders on the stator shaft and rotor housing, on the inside of the rotor assembly. It is secured by an inner bearing retainer (ID #11) and an outer bearing retainer (ID #8) on the outside of the assembly. The inner and outer retainers are respectively fastened to the stator shaft and the rotor housing. On the other hand, only the outer race of the bearing ID #13 is secured using a shoulder in the rotor housing and a bearing outer retainer (ID #10). The lower cage is not secured to enable axial growth of the assembly (onset by thermal stresses). The shaft's ends are splined to ensure that the shaft is secured, against rotation, to the gimbal assembly.
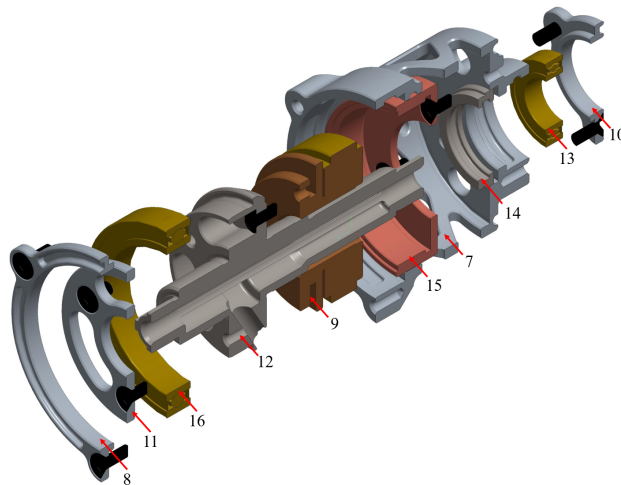
Figure 3.6: Exploded view of rotor assembly

3.1.2 Certain design considerations

The gimbal shaft was custom designed for both structural integrity and minimal weight. It has internal chambers through which the wires to the motor's stator (ID #9) are drawn. Similar channels along the gimbal's housing guide the wires drawn from the slip ring assembly to the stator shaft. The stator shaft (ID #12), like that of the gimbal, consists of internal chambers to guide the wires to the stator windings. These channels have been highlighted in Fig. 3.7. Further, to reduce weight of the rotor and gimbal housings, a webbed structure was adopted while designing the housings. These structures also facilitate air circulation and the consistent cooling of the stator coils. The enclosure frame also consists of holes to vent any heat. Fig. 3.8 displays both aforementioned webbed structures and vent holes.
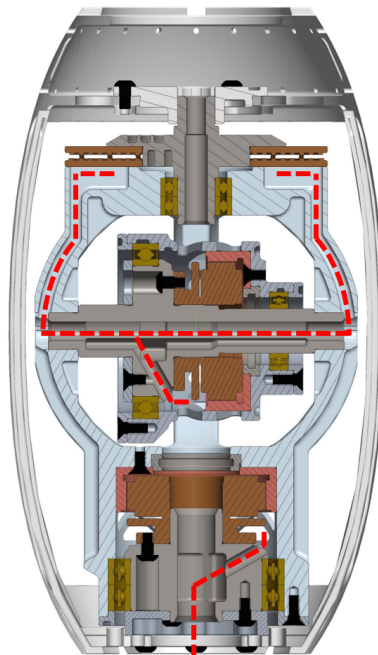
Figure 3.7: Cross sectional view of assembly depicting the channels for wires
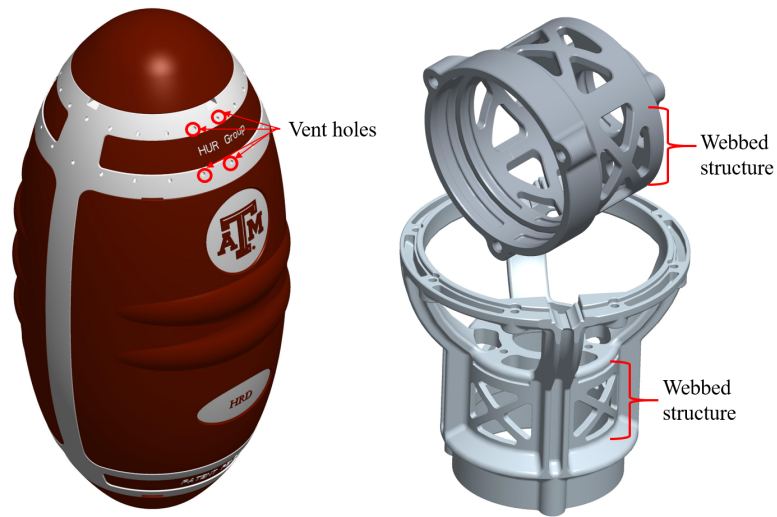
Figure 3.8: Cross sectional view of assembly depicting the channels for wires

3.2 Material selection and manufacturing

In order to minimize the weight, lightweight materials had to be chosen to fabricate the device. Furthermore, the chosen manufacturing process had to have the ability to produce complex and custom geometries. Naturally, additive manufacturing was considered the best and most economical route. Among all additive manufacturing processes, powder bed fusion process was considered most optimal owing to its impeccable resolution and surface finish. Since the components' geometry is complex and has several internal channels, powder bed fusion allowed fabrication without the need for additional support structures. All parts in exclusion of hub locators (ID #14 and #17) were fabricated via 3D printing. As stated earlier, the hub locators were turned on a lathe from a Nylon stock material.

Two major materials were selected for the printing process. Firstly, Alumide (composed of Aluminum particles dispersed in PLA powder) was selected for elements belonging to the rotor assembly. This selection was made based on the higher tensile strength

and density of Alumide compared to PLA [10]. Secondly, PA 2200 (a strong and flexible polymer material) was selected for the all other components. The properties of PA 2200 would allow components to deflect sufficiently in order to be snap fitted into place [10]. The properties of both materials have been provided in Sec. C.1.

3.3 Attestation of structural integrity

A dynamic analysis using Solidworks motion study was conducted to evaluate the stresses induced in the rotor and the gimbal lower housing. For the study, the motion of the rotor and gimbal were prescribed as 300 rad/s and 25 rad/s, respectively. The meshing tool of Solidworks was used to generate fine meshes for both components. Upon processing the dynamics, the results regarding deformations, Von Mises stress, and the corresponding factor of safety were analyzed. A factor of safety greater than 1.5 was considered safe and a validation of the design.

3.4 Biomechanical analysis

This section describes the procedure to evaluate the biomechanical implications of the device. The primary focus was the forces imposed by the device on the hand. These forces will act at every point of the hand in contact with the device. To determine the points of contact, a CAD model of a hand holding the device was built [42]. Fig. 3.9 depicts the built CAD model. Then, information regarding the orientation of each contact point with respect to the center of the object was gathered. If O is the center of the device, then the orientation of a contact point C_i is given by the position vector p_{OC_i} and rotation matrix R_{OC_i} [8]. Fig. 3.9 depicts a contact point C_i located at the thumb and its orientation with respect to the device's center O.
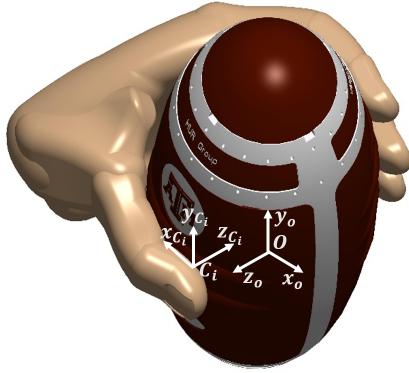
Figure 3.9: CAD model of a hand holding the device

The forces generated by the device at its center can be resolved into a array f_{C_i} at each contact point i. A soft contact model is used to represent the contact between the hand and the device. Each array f_{C_i} is composed of normal force f_z, shear forces f_x and f_y and a torque about the normal direction τ_{z_i} [8].

$$f_{C_i} = \left\{ f_{x_i} \quad f_{y_i} \quad f_{z_i} \quad \tau_{z_i} \right\} \tag{3.1}$$

As per the soft contact model, the components of array f_{C_i} must obey the following inequalities.

$$f_{C_i} \in FC_i$$

$$FC_i = f \in R^4 : \left\{ \begin{array}{c} \sqrt{f_x^2 + f_y^2} \leq \mu f_z \\ f_z \geq 0 \\ |\tau_z| \leq \gamma f_z \end{array} \right\}$$

where μ is the static friction coefficient and γ is the torsional friction coefficient. For the

sake of simplicity, both coefficients are chosen as 0.47, which is the friction coefficient between human skin and Nylon as per [43]. The referenced study included 10 subjects and the stated friction coefficient was determined by studying the shear and normal forces acting at the palm of the hand, while gripping the measuring apparatus.

Furthermore, the array f_{C_i} can be transformed into a vector called contact wrench F_{C_i} using the wrench basis $B_{C_i} \in R^{6 \times 4}$ [8].

$$
F_{C_i} = \begin{bmatrix} 1 & 0 & 0 & 0 \\ 0 & 1 & 0 & 0 \\ 0 & 0 & 1 & 0 \\ 0 & 0 & 0 & 0 \\ 0 & 0 & 0 & 0 \\ 0 & 0 & 0 & 1 \end{bmatrix} f_{C_i}
$$

$$
\implies F_{C_i} = B_{C_i} f_{C_i} \tag{3.2}
$$

The wrench F_{C_i} is then mapped to a wrench acting about the object's center O using the wrench transformation matrix $Ad^T_{g^{-1}_{OC_i}}$.

$$
F_O = \begin{bmatrix} R_{OC_i} & 0 \\ \hat{p}_{OC_i} R_{OC_i} & R_{OC_i} \end{bmatrix} F_{C_i}
$$

$$
\implies F_O = Ad^T_{g^{-1}_{OC_i}} B_{C_i} f_{C_i}
$$

$$
\implies F_O = G_i f_{C_i} \tag{3.3}
$$

$$
\implies G_i = Ad^T_{g^{-1}_{OC_i}} B_{C_i} \tag{3.4}
$$

$G_i \in R^{6 \times 4}$ is the linear map between the contact forces [8]. 19 contact points were iden-

tified via hand CAD model. These points have been illustrated in Fig. 3.10. Note that the convention used to number the digits (or fingers), will be used throughout the sections to follow.
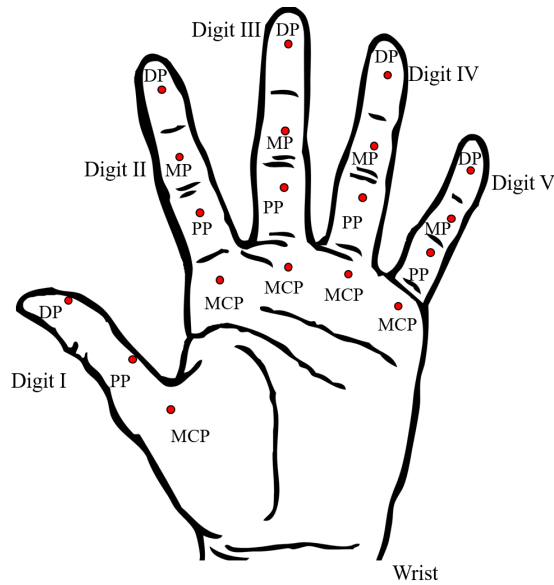
Figure 3.10: Points of contact on the hand. DP – Distal phalanx, MP – Medial Phalanx, PP – Proximal phalanx, MCP – Metacarpal phalanx

A grasp map $G : R^{76} \to R^6$ maps the contact forces acting at each contact point to the total forces acting at the device's center.

$$
F_O = \sum_{i=1}^{19} G_1 f_{C_1} = \begin{bmatrix} G_1 & G_2 & \dots & G_{19} \end{bmatrix} \begin{bmatrix} f_{C_1} \\ f_{C_2} \\ \vdots \\ f_{C_1 9} \end{bmatrix}
$$

$$\implies F_O = G f_C \qquad (3.5)$$

For a given wrench F_O generated by the device, it is desired that the cumulative forces acting on the hand be minimized, while satisfying the constraints to avoid slippage [44]. This can be formulated as an optimization problem as shown.

$$\underset{f_{C_i}}{\text{minimize}} \quad f_C^T f_C$$

$$\text{subject to} \quad G f_C \leq F_O$$

$$f_{x_i}^2 + f_{y_i}^2 \leq (\mu f_{z_i})^2, \quad for \; i = 1, \ldots 19$$

$$\tau_{z_i}^2 \leq (\gamma f_{z_i})^2, \qquad for \; i = 1, \ldots 19$$

$$-f_{z_i} \leq 0, \qquad \quad for \; i = 1, \ldots 19$$

The initial guess for the forces is determined by the solution to Eqn. 3.5 using the pseudo inverse of G. The pseudo inverse, G^+ is found via singular value decomposition.

$$G = USV^T$$

$$G^+ = VS^+U^T$$

where S^+ is found by taking the reciprocal of the non-zero elements in S and performing the transpose of the resulting matrix. All calculations were carried out in Matlab. Sec. C.2 provides the links to access the Matlab codes.

Once the forces acting at each contact point are determined, they can be compared to existing literatures such as [9] and [32] to assess if the they are within safe and operable ranges.

4. RESULTS AND DISCUSSION

The voice of customer and the study of the state of the art served as the customer needs throughout the design process. Based on these needs the target specifications were drafted. It was understood that the HRD can be used quite easily by those who have the ability to grip objects. On the contrary, this might pose a challenge to those who have contracted hand muscles. In such cases, the user would have to use a tensioned glove that would aid in extending fingers and grabbing onto the device.

4.1 Proof of concept

Observations from initial pilot runs revealed that the subject took a few seconds to adjust the grip in accordance to the torque imposed on the hand. The results reported corresponds to the motion of the hand once a stable grip was achieved. Fig. 4.1 presents the results for test 0, that formed the baseline for comparison. Note that the gimbal's speed was given by $6.28\sin(2t)$ rad/s and rotor's speed was 230.38 rad/s. The motion provoked about the pitch and roll axis were equally matched with respect to amplitude. Overall, the generated motion of the hand was periodic, much like the motion of the rotor-gimbal assembly. The repetitive nature of the produced hand motion makes it suitable for rehabilitation. The repeating unit in the response has been highlighted with a red box.
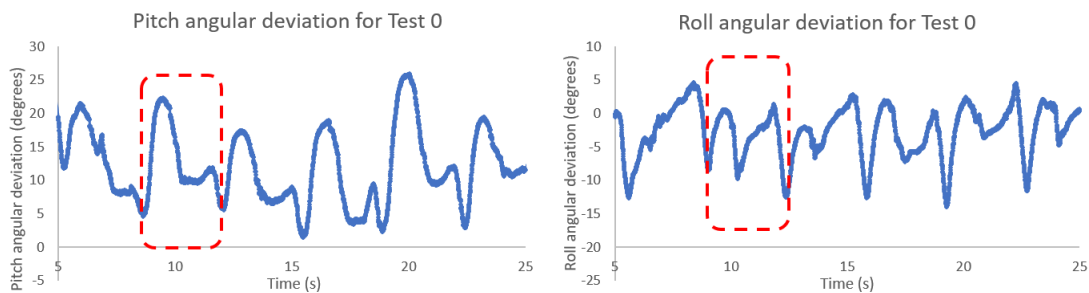
Figure 4.1: Test 0

4.1.1 Varying speed magnitude of gimbal

The results of varying the magnitude of gimbal's speed has been reported in Fig. 4.2 and Fig. 4.3. Note that the magnitude of speed in Test 1.1 was 4.19 rad/s, while the magnitude was 8.38 rad/s in Test 1.2. It was observed that the generated motion was weaker in magnitude when the speed of the gimbal was lowered, in comparison to the baseline. On the other hand, no considerable increase in the hand motion's magnitude was recorded when the speed was increased. But, it was observed that the subject found it harder to maintain a grip about the device when the speed was increased. This inconvenience might have been caused by rotary imbalances or too large of a torque output. It was thus inferred that the speed of the gimbal must be chosen in accordance to the user's ability to tolerate the generated motion.
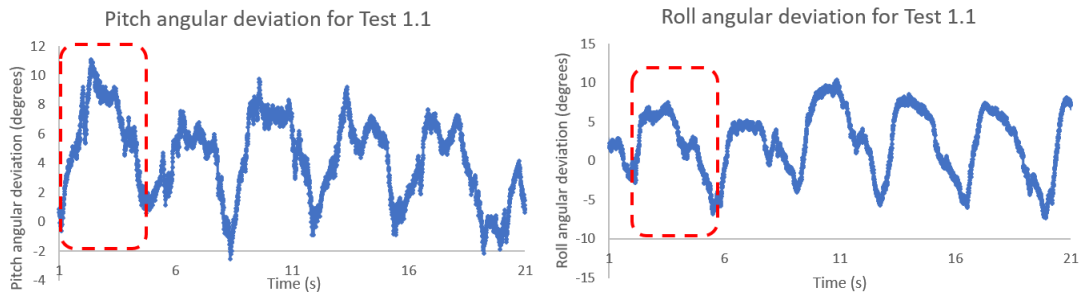
Figure 4.2: Test 1.1
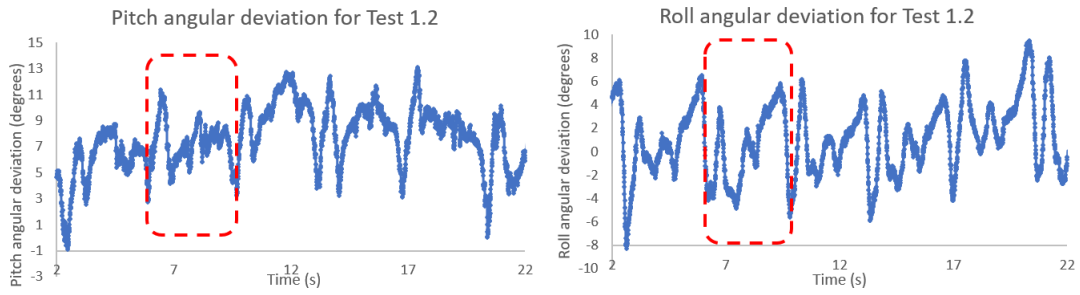
Figure 4.3: Test 1.2

4.1.2 Varying gimbal's period of oscillation

Fig. 4.4 and Fig. 4.5 report the results acquired when the frequency of oscillation was 1.5 rad/s and 2.5 rad/s respectively. It was interesting to note that the frequency of generated hand motion followed that of the gimbal's motion, much like a frequency response of a linear system. Further, the displacements about the pitch axis was more irregular in Test 2.1 compared to the motion observed at higher frequencies. This implies that the frequency of oscillation can be varied to produce different types of hand motion and various regimes of rehabilitation therapy.
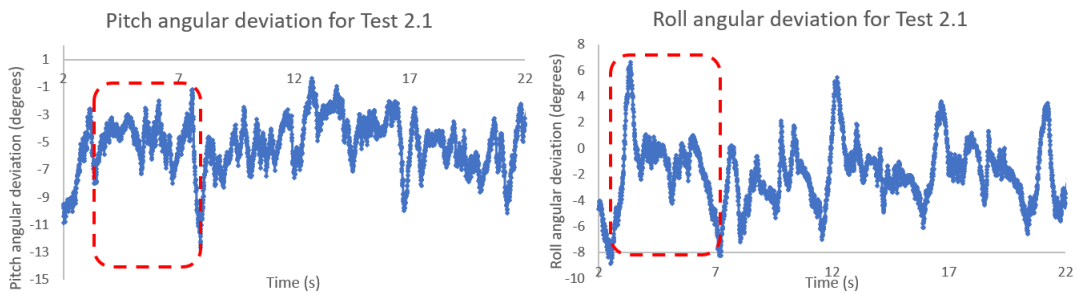
Figure 4.4: Test 2.1
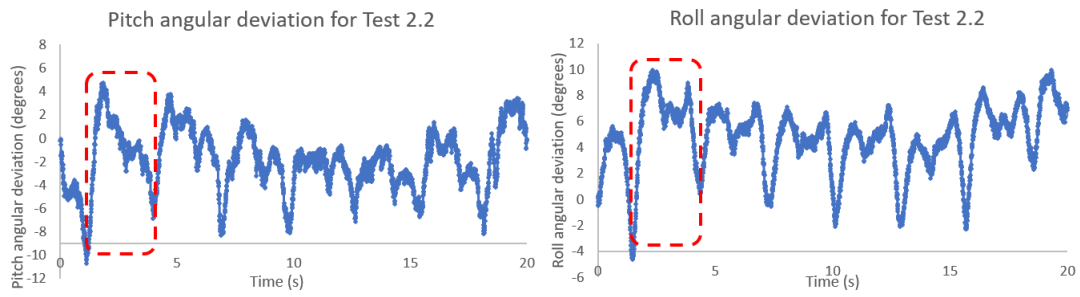
Figure 4.5: Test 2.2

4.1.3 Varying rotor's speed

The recorded results for the generated hand motion when the rotor speed was 136.14 rad/s and 324.63 rad/s has been shown in Fig. 4.6 and Fig. 4.7 respectively. It was observed that variation in the rotor's speed did not affect the magnitude of the angular deflections of the hand. But, the motion about the pitch axis was more irregular when the rotor speed was increased, suggesting that the user faced difficulty in adjusting to the imposed motion.

Figure 4.6: Test 3.1

43
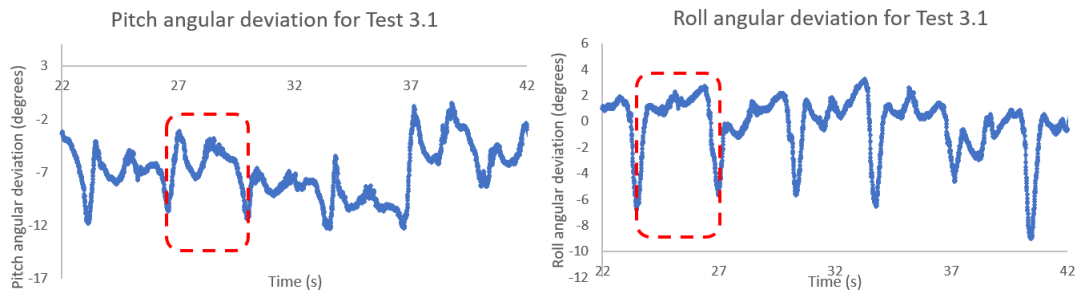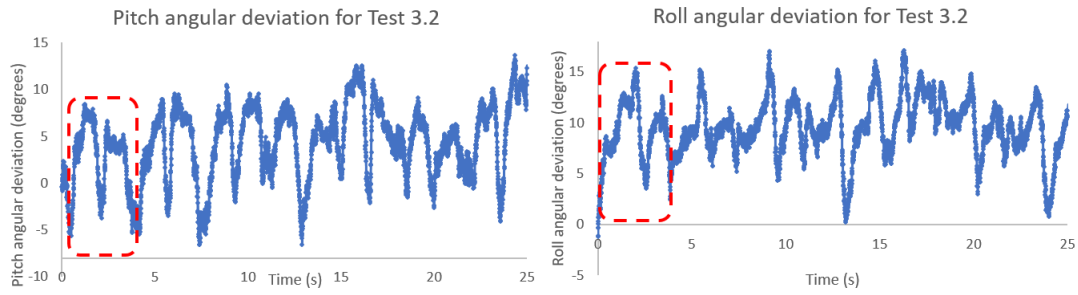
Figure 4.7: Test 3.2

4.2 Summary of final design

The final design weighs about 535.525 g and is a portable device. Given the novelty of the device, a patent application – US Patent Application: 62/413,130, has been filed. An attempt was made to estimate the torques generated by the new device. Unfortunately, there were issues in compiling and deriving the final equations of motion. A major issue was the mass matrix being too close to singularity. Hence, the output torques were determined using the model built in Simscape, a Mathworks simulation software. As per the built simulation, the torques that can be produced by the device have been reported in Fig. 4.8. The torque about the pitch and roll axis have an amplitude of 0.3 Nm.
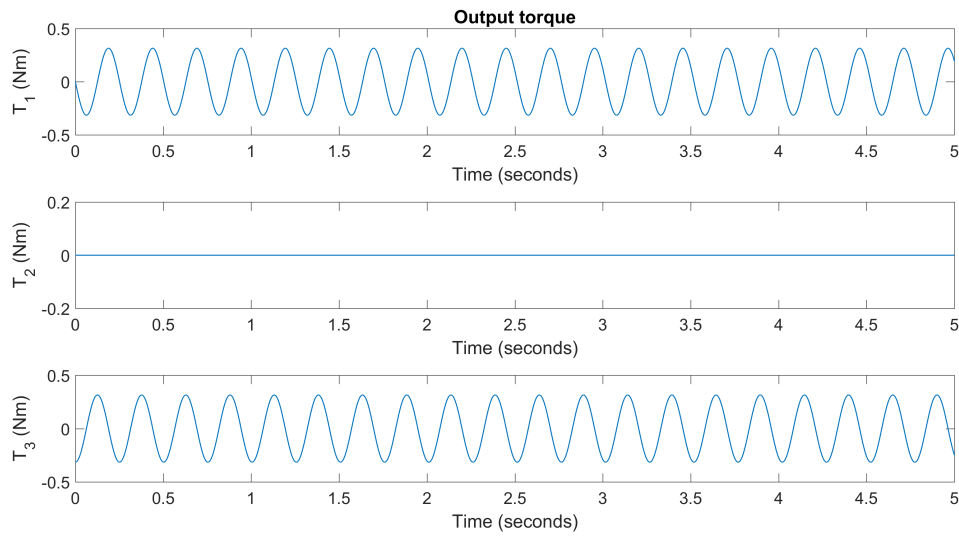
Figure 4.8: Output torque of final design

The torque produced can be increased using heavier materials for the rotor housing. But, by doing so, the weight of the device also increases. Fig. 4.9 and Fig. 4.10 are there resulting torques for an Aluminum and Steel housing respectively. A torque amplitude of 0.73 Nm was achieved with a steel housing. Although the magnitude of the torque matches that stated in the target specifications. But, weighing in at about 644.866 g, it fails to meet the weight requirement. Note that these results were arrived at by direct density replacement of the subject materials without an optimization of form or size. The inertia of the rotor can also be increased by mounting rings made of high density material such as Tungsten heavy alloys [45].
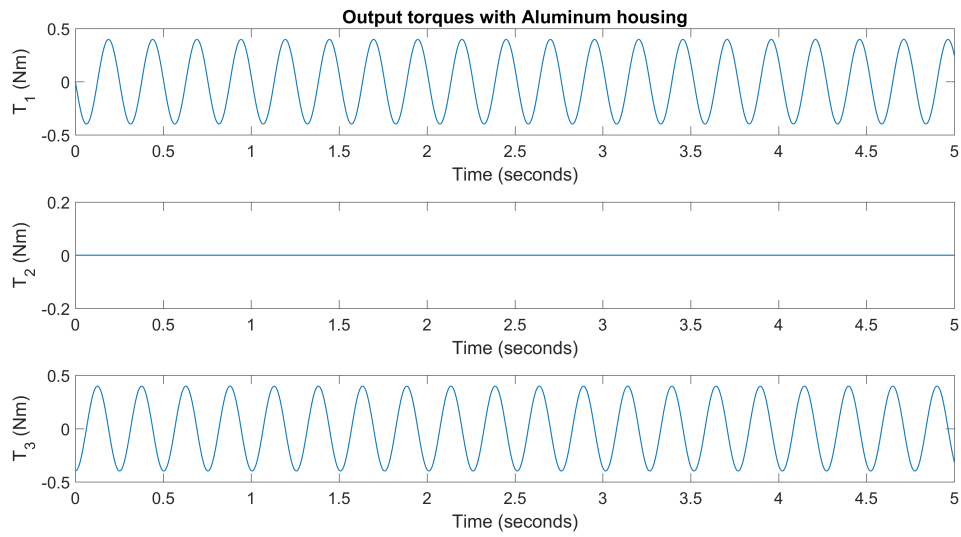
Figure 4.9: Output torque if the design has an Aluminum rotor housing
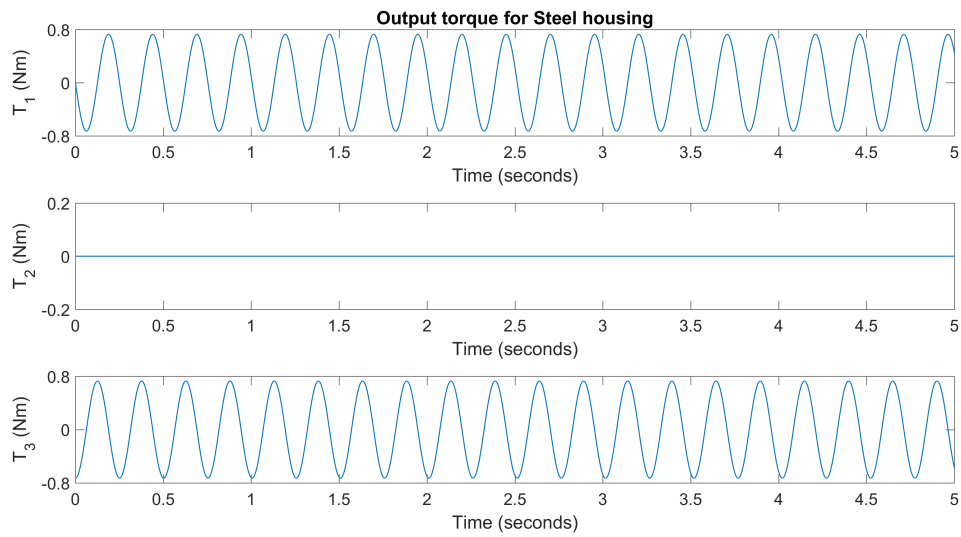
Figure 4.10: Output torque if the design has a Steel rotor housing

4.3 Design analysis

The results of the structural analysis (discussed in Sec. 3.3) have been detailed in this section. Fig. 4.11 depicts the results for the rotor housing. Note that the material of the rotor housing was selected to be Alumide. The Von Mises plot revealed that a maximum stress of 2.217 MPa acts at the region where the housing is secured to the outer bearing retainer (ID #22). The corresponding factor of safety was 32.48 – serving as an exceedingly satisfactory stamp of structural validity. Finally, the deformations plot showed a maximum deflection of 0.136 mm around the point of maximum stress.

(a) Von Mises stress (N/m^2)

(b) Factor of safety

(c) Deformation (mm)
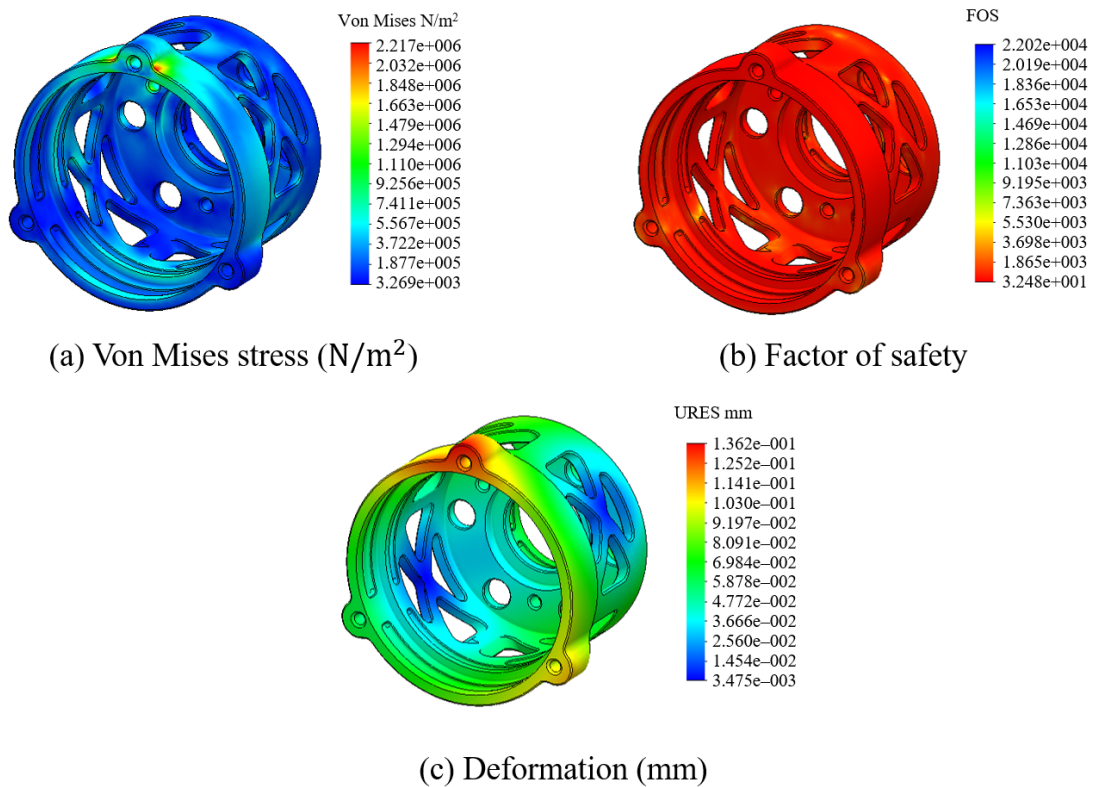
Figure 4.11: Dynamic analysis of the rotor housing

Fig. 4.12 depicts the results for the gimbal lower housing. The maximum Von Mises stress induced in the gimbal housing was 9.384 MPa and the corresponding factor of safety was 6.181. It can thus be concluded that the gimbal can be safely operated at the specified input conditions. The maximum deflection observed was 0.266 mm around the upper rim of the housing.

(a) Von Mises stress (N/m^2)

(b) Factor of safety

(c) Deformation (mm)
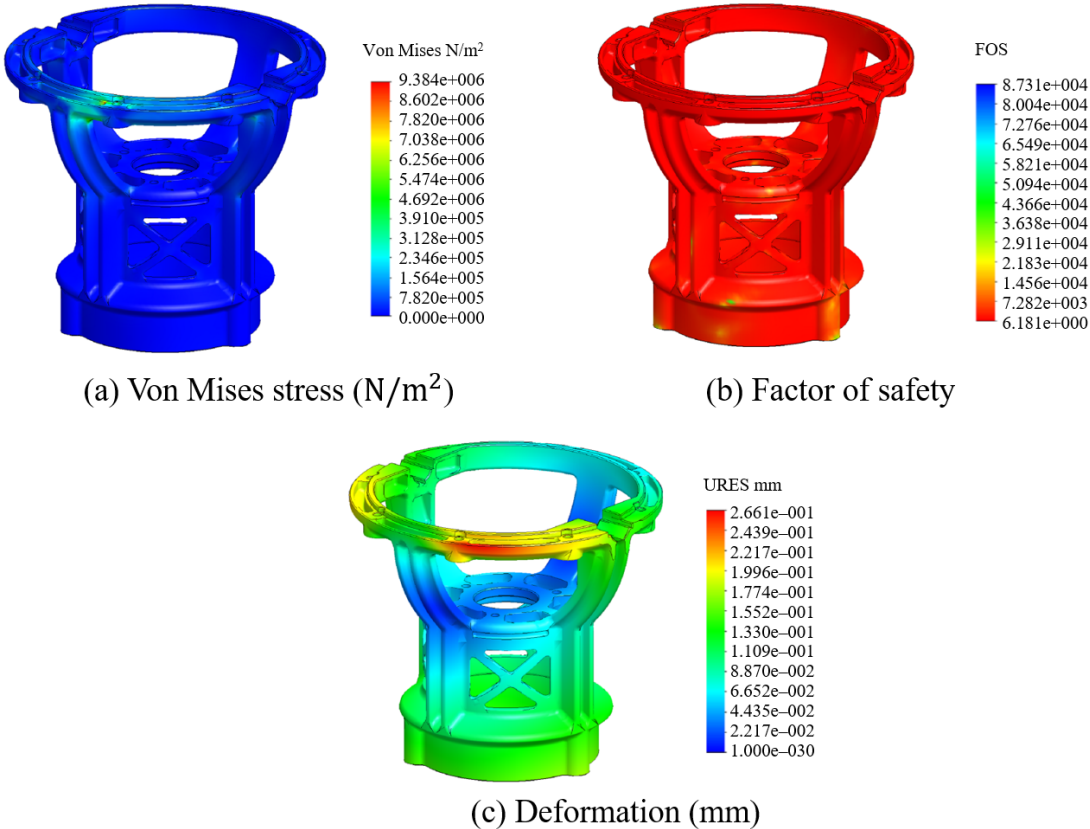
Figure 4.12: Dynamic analysis of the gimbal

4.4 Biomechanical analysis

This section presents the results of optimization problem outlined in Sec. 3.4. The total forces/torques generated by the device, F_O, are resolved into forces acting at each contact point on the hand. As stated earlier a torque of 0.7 Nm is the output torque desired from the device. Hence the wrench F_O is assumed to be composed of 0.7 Nm about the device's pitch and roll axis. The configuration of the axis is such that the gravitational component acts along the yaw axis. The weight of the device (5.2535 N), acting along the yaw axis, is also factored into F_O.

$$F_O = \left\{ 0 \quad -5.2535 \quad 0 \quad 0.7 \quad 0 \quad 0.7 \right\} \tag{4.1}$$
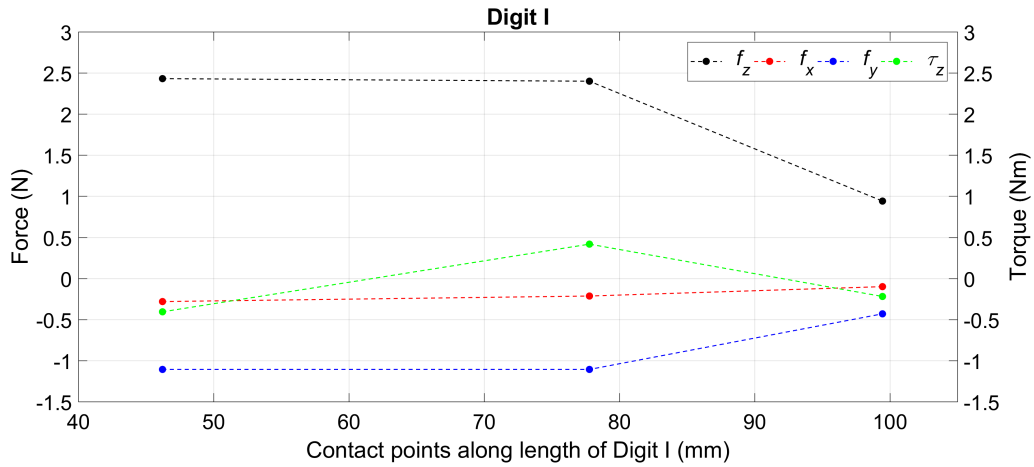
Figure 4.13: Contact wrench components acting on digit I
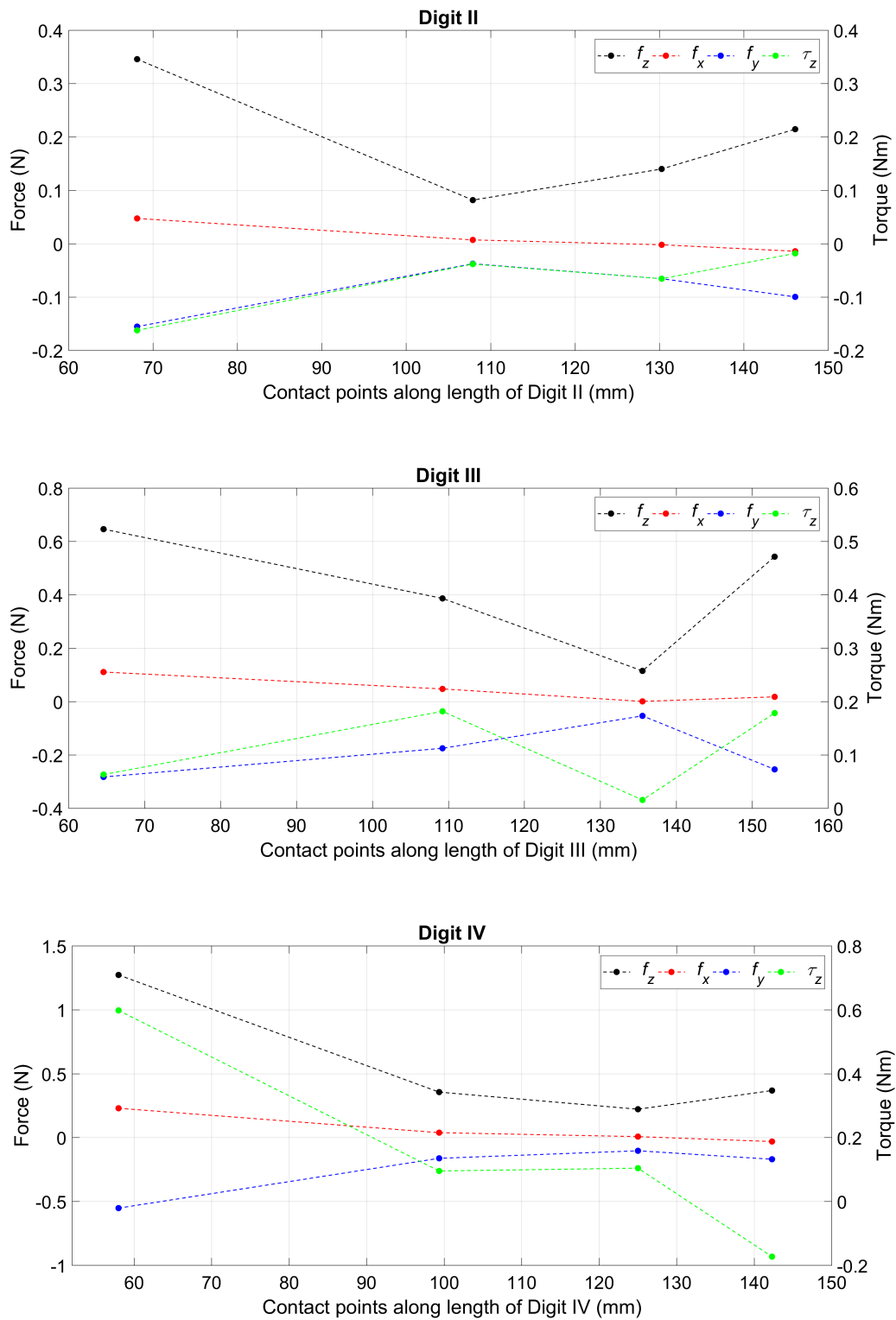
Figure 4.14: Contact wrench components acting on digit II, III and IV
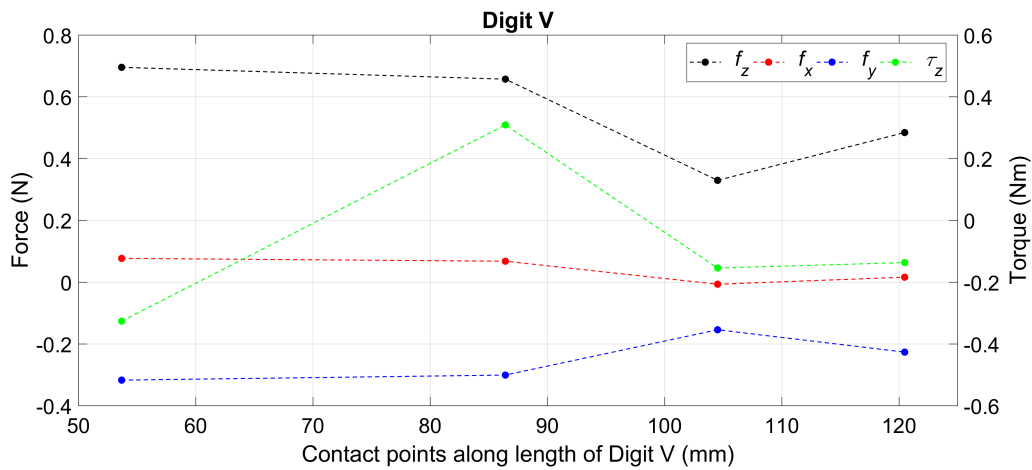
Figure 4.15: Contact wrench components acting on digit V

The produced results satisfied all the constraints in order to maintain a grip about the device. Specifically, the shear forces and contact torque are such that slippage is avoided.

As expected, the majority of the normal force acts on the metacarpal phalanx, except in the case of Digit I. This could be due to the fact that the metacarpal phalanx of Digit I had minimal contact with the device compared to the other phalanxes. With regard to the trend observed in the distribution of normal forces, these results differed from those presented in [9] and [32], where the force imposed by the distal phalanx was greater than that acting on the other two phalanxes (not including the metacarpal phalanx). Note that both references do not record the forces acting on the metacarpal phalanxes, which could be one of the reasons behind the discrepancies. Additionally, both references investigate static power grips (the maximum force an individual can impose) and result in total normal forces greater than 100 N; far higher than those resulting from the HRD. The total normal force imposed by the HRD was calculated to be 12.62 N.

51

Percentage contribution of each finger to total force
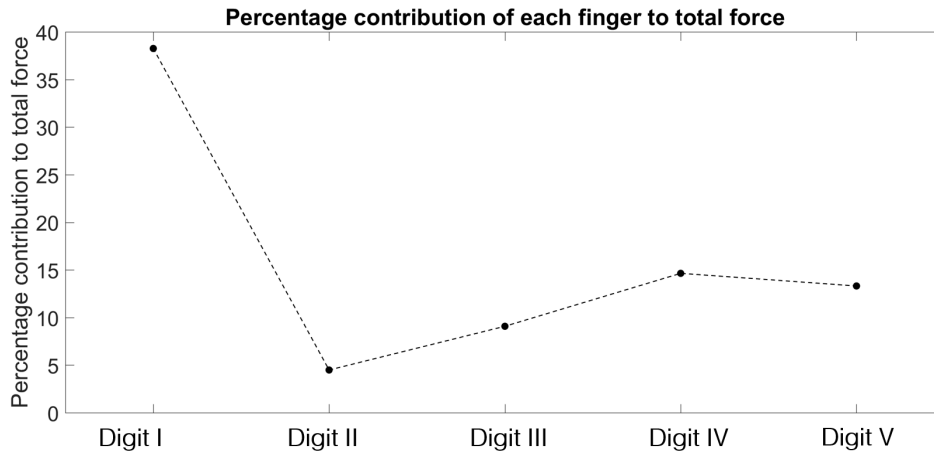
Figure 4.16: Contribution of each finger to the total normal force

Upon analyzing the percentage contribution for each finger to the total normal force, it is inferred that Digit I contributes the most, followed by the other digits. The percentage contribution varied from that presented in Fig. 1.7 in terms of both magnitude and trend. This can be explained by comparing the orientation of the fingers. This comparison has been presented in Fig. 4.17. The study [32] recorded that the contact forces imposes by the hand vary with the size of the cylinder being gripped. This is primarily due to change in the orientation and position of each finger. Similarly, unlike [9] where Digit I was at the same level as Digit II, the study involving the HRD places Digit I between Digit III and Digit IV. These changes in finger orientation highly contributes towards the lower force contribution of Digit II. Further, the difference in the trend of percentage contribution can be attributed to the fact that the HRD is an ellipsoid with finger grooves, while the object gripped in [9] was a cylindrical. Also, the fact that [9] studied a power grip, unlike the case with HRD, contributes to the observed discrepancies. Hence, it was inferred that the HRD can operated safely by stroke patients. The current finger grooves can be redesigned to generate a percentage force contribution similar to that reported in [9] and [32].

52

Figure 4.17: The grip implemented in the study regarding the HRD

5. SUMMARY AND CONCLUSIONS

This thesis proposes a novel hand-held, gyroscopic device that forces the user's hand to move by imposing a torque. A proof-of-concept model showed that the resultant hand motion is periodic and can be altered in magnitude and frequency by controlling the gimbal's motion. The passive and repetitive movement of the hand, as dictated by gyroscopic torque, can result in muscle relaxation and in turn combat hand spasticity. If the user actively resisted the hand motion, it could increase muscle strength and coordination. But, patients with constantly flexed fingers would experience difficulties in gripping the device. Such patients would have to use a tensioned glove (for instance the Saebo glove) to facilitate finger extension.

Weighing about 536 g the HRD will not only enable in-home rehabilitation, owing to portable nature, it will also allow patients undergo rehabilitation anywhere and at any time. Therefore, patients would have to pay lesser visits to therapy centers. The final design is believed to be capable of producing torques of 0.6 Nm (peak-to-peak value). The magnitude of the torque can be increased by changing the material of the rotor housing or by fitting rings of high density materials (such as Tungsten heavy alloys [45]), targeting a higher inertia, but not necessarily increasing the mass.

The dynamical analysis of the device estimated the stresses induced in the device's primary components and consecutively attested the structural integrity of the device. Further, a biomechanical analysis was conducted by simulating the forces imposed on the hand. It was revealed that the device can impose a maximum total normal force of 8.98 N. On comparing the results regarding force distribution with existing literatures, it was inferred that the device would be safe to operate by those with disabilities.

Further, the device's sportive look could potentially make therapy fun and consecu-

tively accelerate the rehabilitation process. In acknowledgment of its novel design, a provisional patent (US Patent Application: 62/413,130) has been acquired. Finally, the device will be renamed as *"Gymball"*, in reference to the device's sportive nature, its resemblance to a football, and a major component of the device – the gimbal. The football look increases the user appeal of the device and can motivate patients to carry out rehabilitative exercises.

5.1   Further Study

Certain elements that are still undergoing design include the electronic system and the satchel that will house the electrical system. The bag will also have a provision for the mechanical assembly to stowed when not in use. Additionally, since the assembly consists of high precision parts, a safety cable will be attached to the assembly's enclosure frame to prevent accidental drops. This cable is then attached to a belt/cuff that wraps around the user's wrist.

Further, the device will be fabricated and its performance will be evaluated experimentally with human subjects. Like any rehabilitation process, there is a need to assess the user's progress. To do so, a method to quantify the performance of the user must be established. One possible technique would be to measure the hand's angular displacements using a Motion Processing Unit mounted on the hand. These displacements can then be recorded in a system and compared with prior recorded data to determine if the user's range of motion has improved. Other tools that can be used to evaluate the outcome of the experiments include: (i) Fugl-Meyer assessment – to study the change in range of motion and motor function [46], (ii) Modified Ashworth Scale (MAS) – used as a measure of spasticity [47], (iii) Electromyography (EMG) signals – in order to observe the level of muscle activation [15]. Prior to carrying out studies with human subjects, appropriate regulations such as those imposed by the IRB will be staunchly followed. In addition, details such as

the classification of the device as per FDA definition of medical devices will be studied. These details will further establish regulations that the device must conform to in order to be successfully launched in the market.

In addition to the final device, a tensioned glove will be developed for patients with a weakened ability to grasp objects. The tensioning mechanism would combat the resistance offered by muscle contractions and aid in overcoming low grip strength.

5.2   Impact of thesis

The Gymball is expected to lay the foundation for derivative therapeutic products catering to specific needs of the consumers. The targeted customers would include stroke victims, patients with Arthritis, Carpal Tunnel Syndrome, and those recovering from hand injuries/surgeries. Currently, the Texas A&M Technology Commercialization department is seeking potential investors for the Gymball. It is strongly believed that the device's technology can unlock the potential of therapeutic hand devices to be compact and portable.

REFERENCES

[1] Saebo, "Saeboglove." from URL `https://www.saebo.com/saeboglove/`.

[2] Flint Rehabilitation Devices, "Musicglove." from URL `https://www.flintrehab.com/musicglove/`.

[3] Atlas of the future, "Exo-glove-poly." from URL `http://atlasofthefuture.org/project/`.

[4] GyroGear, "Gyroglove." from URL `http://gyrogear.co/gyroglove`.

[5] NSD, "Sports, injury fitness and rehabilitation training aid | powerball." from URL `https://powerballs.com/`.

[6] K. T. Ulrich and Steven D. Eppinger, *Product Design and Development*. Irwin/McGraw-Hill, 5th edition ed., 2011.

[7] W. E. King, A. T. Anderson, R. M. Ferencz, N. E. Hodge, C. Kamath, S. A. Khairallah, and A. M. Rubenchik, "Laser powder bed fusion additive manufacturing of metals; physics, computational, and materials challenges," *Citation: Applied Physics Reviews*, vol. 2, 2015.

[8] R. M. Murray, Z. Li, and S. S. Sastry, *A Mathematical Introduction to Robotic Manipulation*, vol. 29. CRC Press, 1994.

[9] L. R. Enders, *Role of Sensation in Altered Phalanx Grip Force in Persons with Stroke*. Theses and dissertations, University of Wisconsin Milwaukee, 2014.

[10] Shapeways, "3D Printing Materials: Plastic, Metal, Ceramics and More - Shapeways." from URL `https://www.shapeways.com/materials`.

[11] W. Penfield, *The cerebral cortex of man : a clinical study of localization of function*. New York :: Macmillan, 1950.

[12] The internet stroke center, "Stroke statistics." from URL `http://www.strokecenter.org/patients/`.

[13] B. H. Dobkin, "Rehabilitation after Stroke," *The New England Journal of Medicine*, vol. 352(16), pp. 1677–1684, 2005.

[14] G. Kwakkel, B. J. Kollen, J. V. Van der Grond, and A. J. H. Prevo, "Probability of regaining dexterity in the flaccid upper limb: Impact of severity of paresis and time since onset in acute stroke," *Stroke*, vol. 34, no. 9, pp. 2181–2186, 2003.

[15] M. O. Conrad, D. G. Kamper, S. Kang, S. Chun, J. Shin, T. Khalil, and et Al., "Isokinetic strength and power deficits in the hand following stroke.," *Clinical neurophysiology : official journal of the International Federation of Clinical Neurophysiology*, vol. 123, pp. 1200–6, jun 2012.

[16] A. Heller, D. T. Wade, V. A. Wood, A. Sunderland, R. Langton Hewer, and E. Ward, "Arm function after stroke: measurement and recovery over the first three months," *Journal of Neurology Neurosurgery, and Psychiatry*, vol. 50, pp. 714–719, 1987.

[17] N. P. O'Dwyer NJ, Ada L, "Spasticity and muscle contarcture following a stroke," *Brain*, vol. 119, pp. 1737–49, 1996.

[18] Centers for Disease Control and Prevention, "Osteoarthritis Fact Sheet," 2017. from URL `https://www.cdc.gov/arthritis/basics/osteoarthritis.htm`.

[19] M. J. Concannon, M. L. Brownfield, and C. L. Puckett, "The incidence of recurrence after endoscopic carpal tunnel release.," *Plastic and reconstructive surgery*, vol. 105, pp. 1662–5, apr 2000.

[20] R. L. Gajdosik, D. W. Vander Linden, A. K. Williams, and A. Chaparro, Michael Rogers, Jeffrey F, "Range of motion of the wrist: implications for designing computer input devices for the elderly," *Physical therapy*, vol. 22, no. 9, pp. 827–38, 1999.

[21] C. Bütefisch, H. Hummelsheim, P. Denzler, and K. H. Mauritz, "Repetitive training of isolated movements improves the outcome of motor rehabilitation of the centrally paretic hand," *Journal of the Neurological Sciences*, vol. 130, no. 1, pp. 59–68, 1995.

[22] S. P. Shah SK, Harasymiw, "Stroke rehabilitation: Outcome based on Brunnstrom Recovery Stages," *The Occupational Therapy Journal of Research*, vol. 6, pp. 365–376, 1986.

[23] L. M. Kuchinke and B. Bender, "Technical view on requirements for future development of hand-held rehabilitation devices," *Proceedings of the IEEE RAS and EMBS International Conference on Biomedical Robotics and Biomechatronics*, vol. 2016-July, pp. 804–809, 2016.

[24] H. In, B. B. Kang, M. K. Sin, and K. J. Cho, "Exo-Glove: A wearable robot for the hand with a soft tendon routing system," *IEEE Robotics and Automation Magazine*, vol. 22, no. 1, pp. 97–105, 2015.

[25] T. Petrič, B. Curk, P. Cafuta, and L. Žlajpah, "Modelling of the robotic Powerball®: a nonholonomic, underactuated and variable structure-type system," *Mathematical and Computer Modelling of Dynamical Systems*, vol. 16, no. 4, pp. 327–346, 2010.

[26] E. Seabra, L. F. Da Silva, P. Flores, J. Machado, M. H. Vu, M. Martins, and R. Campos, "Mechatronic medical device for wrist rehabilitation," *IEEE International Conference on Industrial Informatics (INDIN)*, pp. 331–336, 2013.

[27] K. Gadd, *TRIZ for engineers : enabling inventive problem solving*. Wiley, 2011.

[28] N. Smania, A. Picelli, D. Munari, C. Geroin, P. Ianes, A. Waldner, and M. Gandolfi, "Rehabilitation procedures in the management of spasticity," *European Journal of Physical and Rehabilitation Medicine*, vol. 46, no. 3, pp. 423–438, 2010.

[29] G. Sequeira, J. W. Keogh, and J. J. Kavanagh, "Resistance training can improve fine manual dexterity in essential tremor patients: A preliminary study," *Archives of Physical Medicine and Rehabilitation*, vol. 93, no. 8, pp. 1466–1468, 2012.

[30] S. Y. Liang and A. J. Shih, *Analysis of Machining and Machine Tools*. Springer, 2016.

[31] I. Gibson, D. D. W. Rosen, and B. Stucker, *Additive Manufacturing Technologies: Rapid Prototyping to Direct Digital Manufacturing*, vol. 54. Springer US, 2009.

[32] A. A. Amis, "Variation of finger forces in maximal isometric grasp tests on a range of cylinder diameters," *Journal of Biomedical Engineering*, vol. 9, no. 4, pp. 313–320, 1987.

[33] J. Case-Smith, "Outcomes in Hand Rehabilitation Using Occupational Therapy Services," *American Journal of Occupational Therapy*, vol. 57, pp. 499–506, sep 2003.

[34] O. Lambercy, L. Dovat, R. Gassert, E. Burdet, C. L. Teo, and T. Milner, "A haptic knob for rehabilitation of hand function," *IEEE Transactions on Neural Systems and Rehabilitation Engineering*, vol. 15, no. 1, pp. 356–366, 2007.

[35] T. Hirsch, J. Forlizzi, E. Hyder, J. Goetz, C. Kurtz, and J. Stroback, "The ELDer project," in *Proceedings on the 2000 conference on Universal Usability - CUU '00*, (New York, New York, USA), pp. 72–79, ACM Press, 2000.

[36] J. J. Uicker, G. R. Pennock, and J. E. Shigley, *Theory of machines and mechanisms*. Oxford University Press, 2011.

[37] J. Rowberg, "I2C Device Library." from URL
`https://www.i2cdevlib.com/`.

[38] A. Palmer, F. Werner, D. Murphy, and R. Glisson, "Functional wrist motion: a biomechanical study," *The Journal of hand surgery*, vol. 10, no. 1, pp. 39–46, 1985.

[39] Spong, "Robot dynamics and control," *Automatica*, vol. 28, no. 3, pp. 655–656, 1992.

[40] Wolfram, "Robotica: A mathematica package for robot analysis." from URL
`http://library.wolfram.com/infocenter /Articles/999/`.

[41] C. Lin and J. F. Tu, "Model-Based Design of Motorized Spindle Systems to Improve Dynamic Performance at High Speeds," *Journal of Manufacturing Processes*, vol. 9, pp. 94–108, jan 2007.

[42] Joerg Schmit, "human left hand - 3D CAD model - GrabCAD." from URL
`https://grabcad.com/library/human-left-hand`.

[43] M. Zhang and A. F. T. Mak, "In vivo friction properties of human skin," *Prosthetics and Orthotics International*, vol. 23, pp. 135–141, 1999.

[44] R. Tomovic, G. Bekey, and W. Karplus, "A strategy for grasp synthesis with multifingered robot hands," *Proceedings. 1987 IEEE International Conference on Robotics and Automation*, vol. 4, pp. 83–89, 1987.

[45] Plansee, "Tungsten heavy metal | Plansee." from URL
`https://www.plansee.com/en/materials`.

[46] V. Squeri, L. Masia, P. Giannoni, G. Sandini, and P. Morasso, "Wrist rehabilitation in chronic stroke patients by means of adaptive, progressive robot-aided therapy," *IEEE Transactions on Neural Systems and Rehabilitation Engineering*, vol. 22, no. 2, pp. 312–325, 2014.

[47] J. M. Gregson, M. Leathley, A. Moore, A. K. Sharma, T. L. Smith, and C. L. Watkins, "Reliability of the tone assessment scale and the modified ashworth scale as clinical tools for assessing poststroke spasticity," *Archives of Physical Medicine and Rehabilitation*, vol. 80, pp. 1013–1016, sep 1999.

APPENDIX A

LITERATURE REVIEW

The contribution of 4 digits (index – little finger) as per [32] has been shown in the below image.
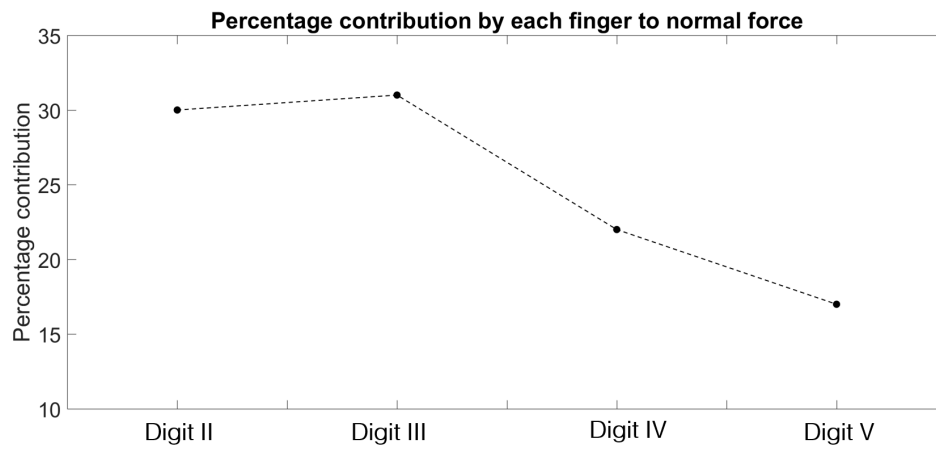
Figure A.1: Contribution of first 4 digits to the total normal force [32]

APPENDIX B

PROOF OF CONCEPT AND MATHEMATICAL MODELING

B.1   Proof of concept

The following sections include schematics of the electrical system, Labview program, and arduino code of the IMU. Finally, the repositories for the simulation code and images of the Simscape model have also been provided.

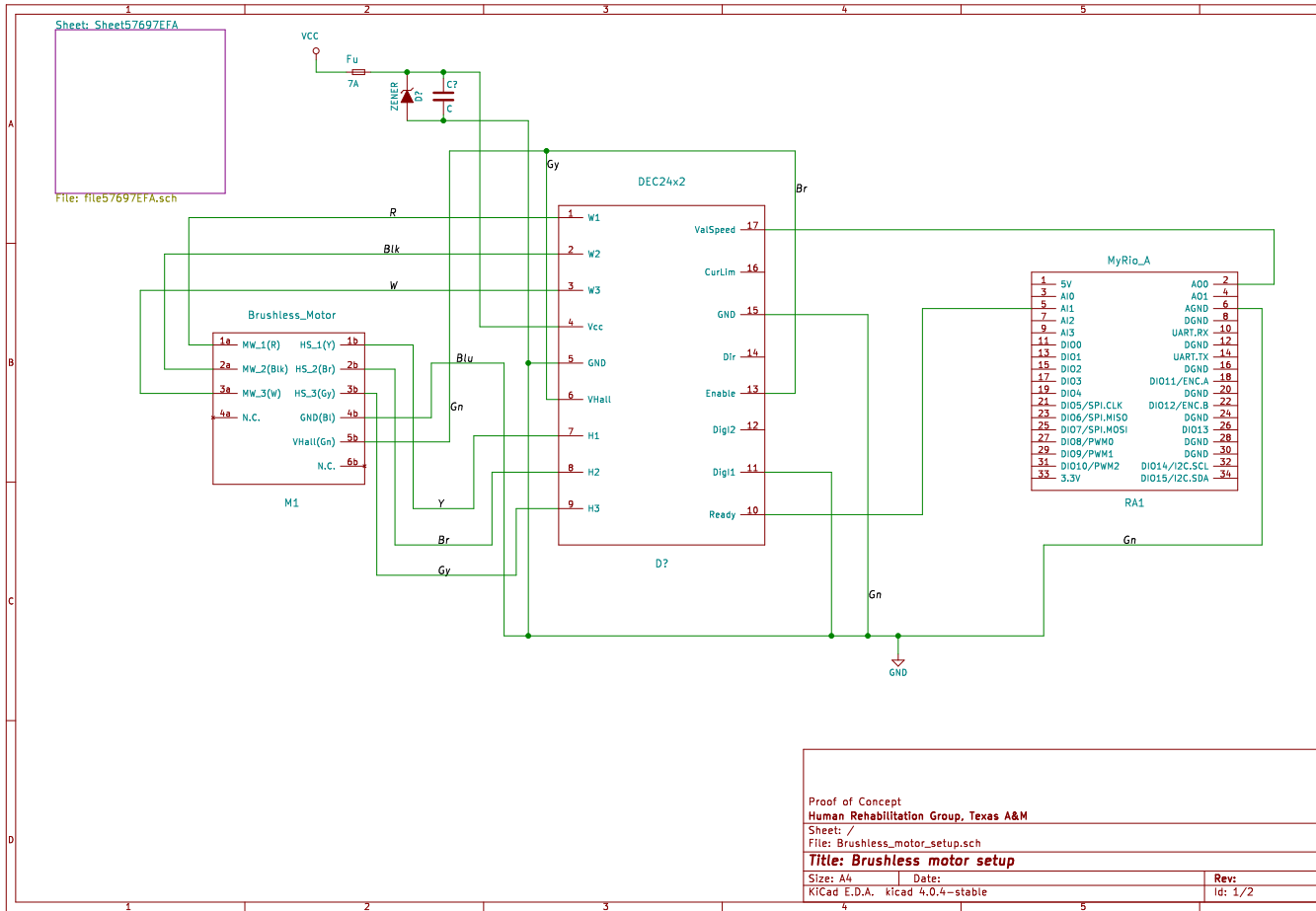### B.1.1 Electrical system for Proof of concept model

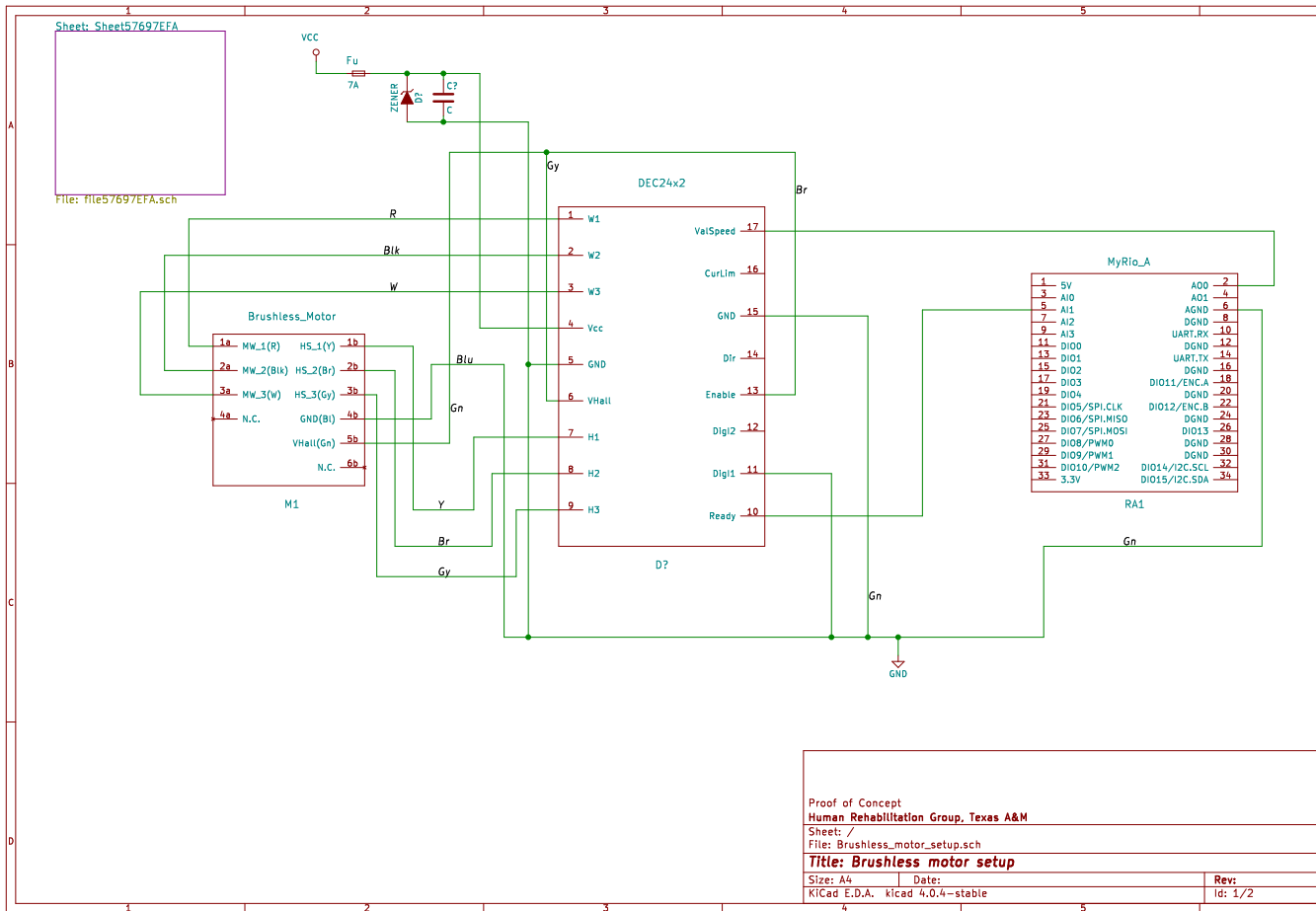Figure B.1: Schematic of electrical set up for brush-less motor

Figure B.2: Schematic of electrical set up for brushed motor

B.1.2 Labview program

Select desired speed for both brushed and brushless motor
For brushed motor   Kp = 1.03   Ki = 1.15

Brushed Motor

Desired speed

| 0 | 20 | 40 | 60 | 80 | 100 | 120 | 140 | 160 | 180 | 190 |

omega

2

Kp

1.03

Ki

1.15

Speed in rpm

0

Counter Value

0

Counter Direction

Counting Up

Brushless motor set value speed

Set value speed voltage

| 0 | 0.5 | 1 | 1.5 | 2 | 2.5 | 3 | 3.5 | 4 | 4.5 | 5 |

error out

status   code

0

source

stop

STOP

Results

| 75 | 50 | 25 | 0 | -25 | -50 | -75 | -100 | -125 | -150 |

0   1023
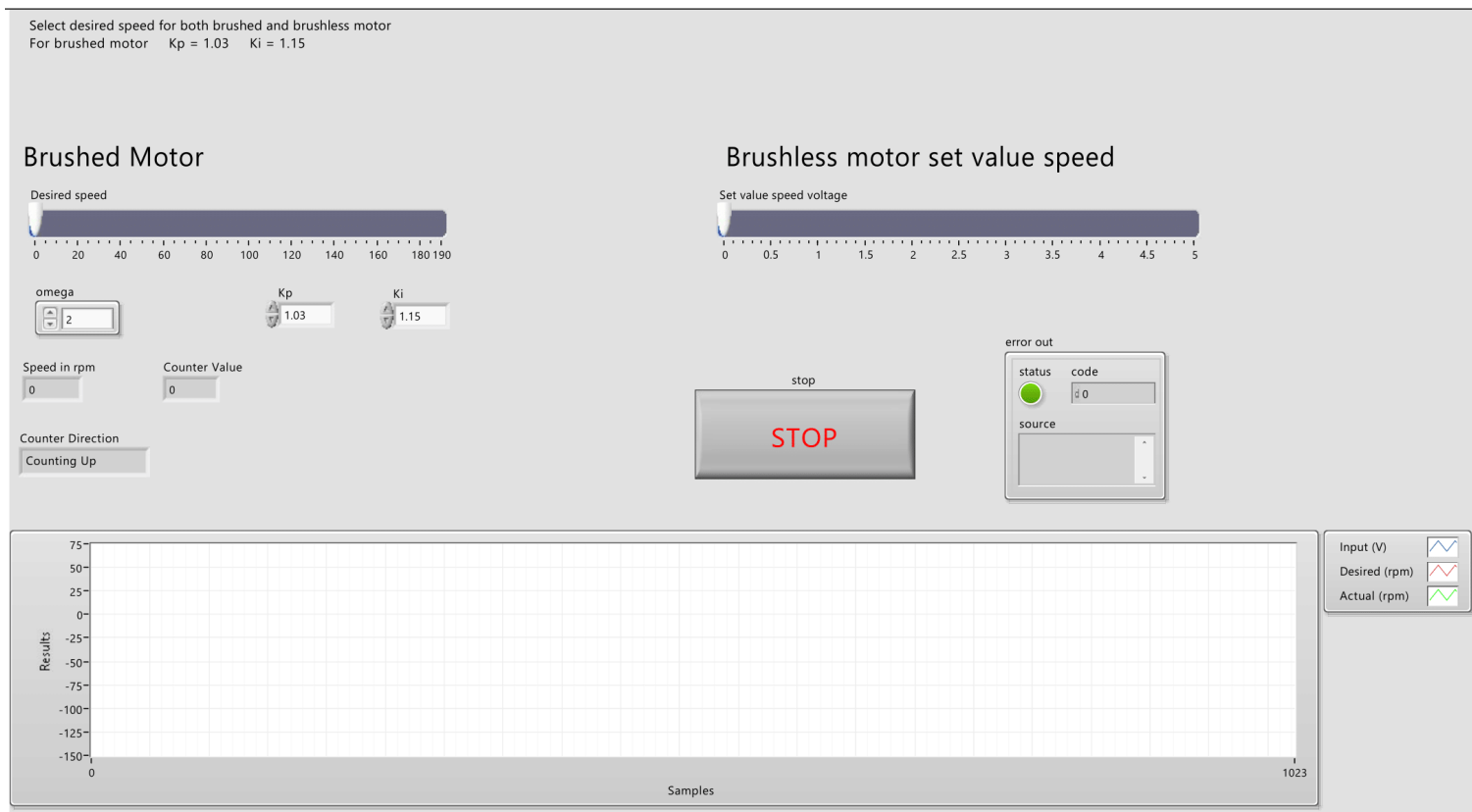
Samples

Input (V)
Desired (rpm)
Actual (rpm)

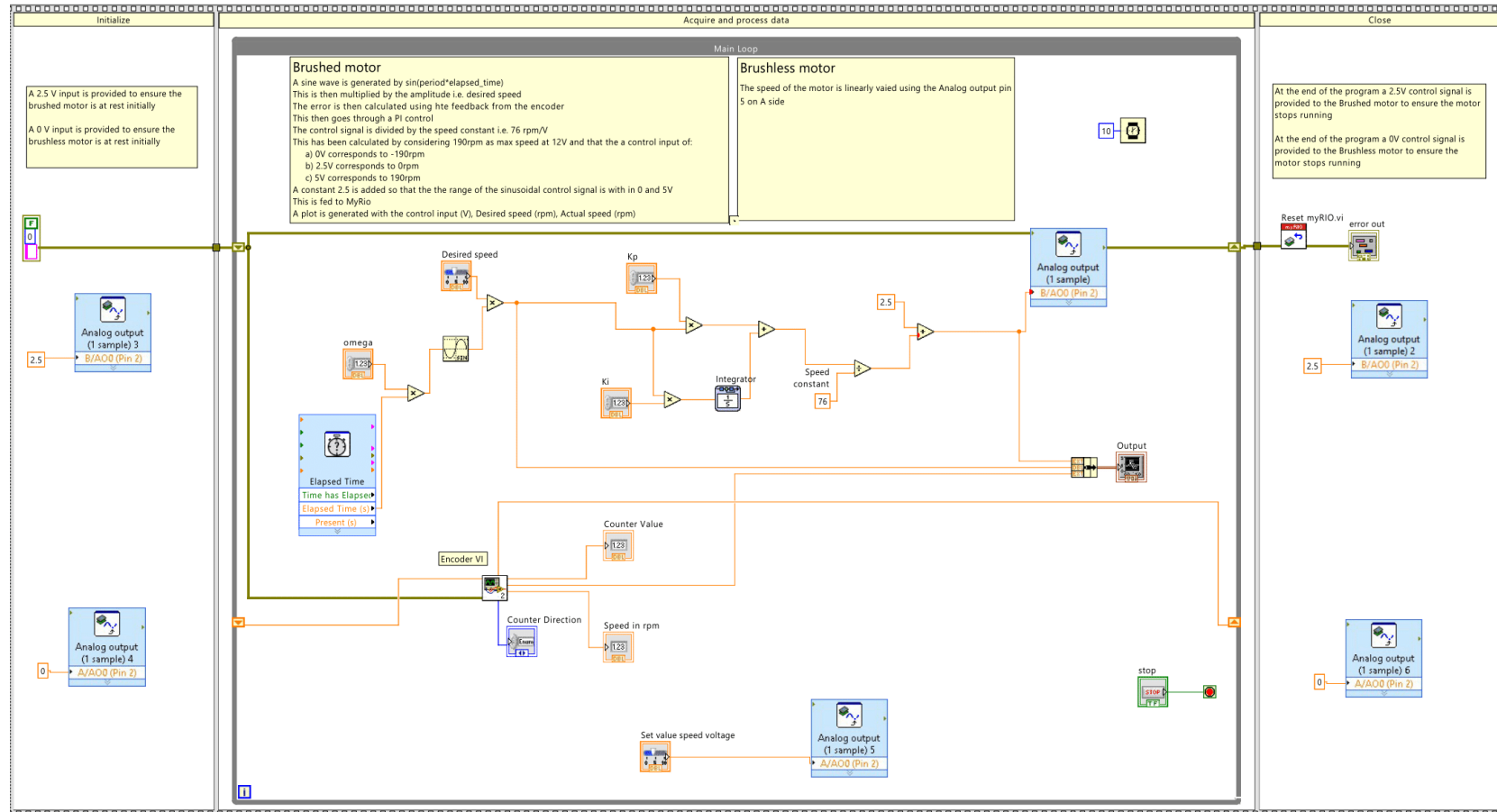Figure B.3: Labview front view of main program
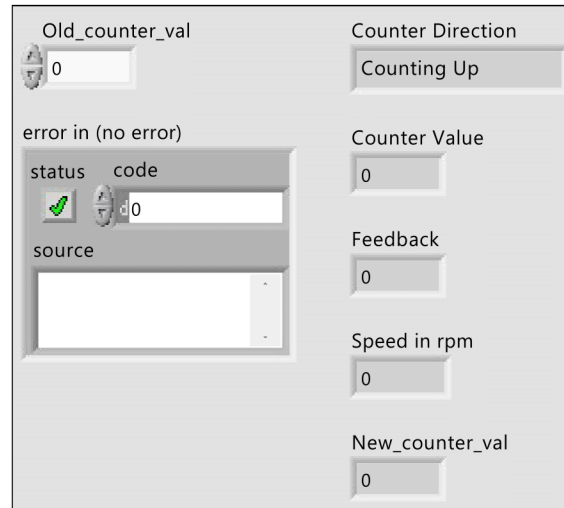
Figure B.4: Labview block diagram of main program

Figure B.5: Labview front view of sub program

The counter value is acquired from MyRio
This is divided by 64 i.e. the counts per revolution
Then divided by 50 which is the gear reduction ratio for the motor
This is further subtracted by the older counter value (previous iteration)
The difference is divided by the loop delay time i.e. 10ms
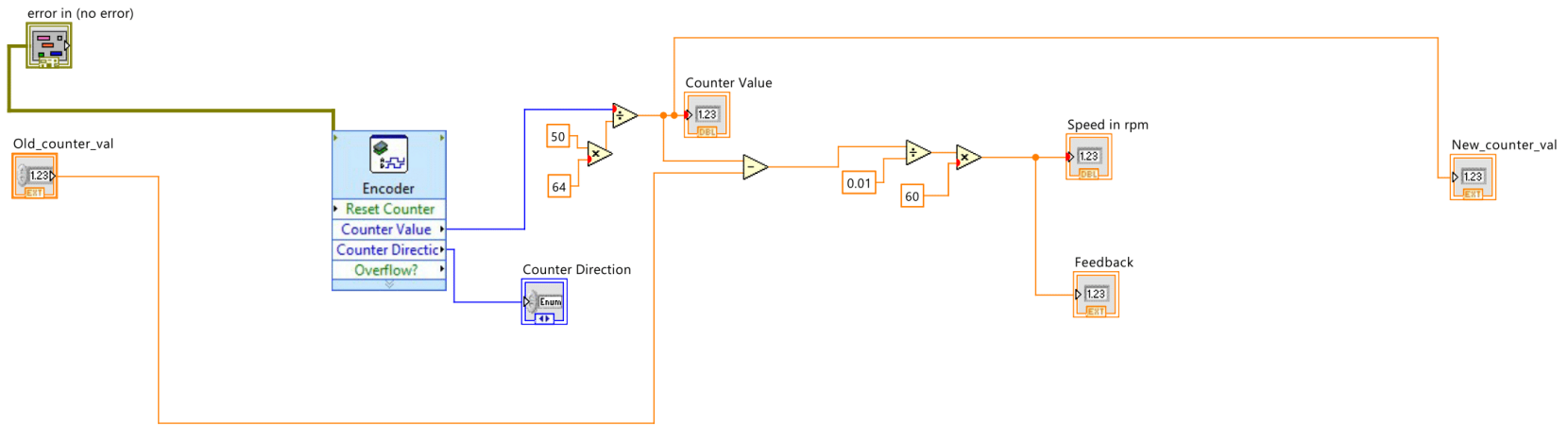Then multiplied by 60s to get the speed in rpm

Figure B.6: Labview block diagram of sub program

B.1.3 Arduino code for motion processing

```
// I2C device class (I2Cdev) demonstration Arduino sketch for
//MPU9150 1/4/2013 original by Jeff Rowberg <jeff@rowberg.net>
//at https://github.com/jrowberg/i2cdevlib
//modified by Aaron Weiss <aaron@sparkfun.com>
//
// Changelog:
//     2011-10-07 - initial release
//     2013-1-4 - added raw magnetometer output


/* =============================================
I2Cdev device library code is placed under the MIT license

Permission is hereby granted, free of charge, to any person
obtaining a copy of this software and associated documentation
files (the "Software"), to deal in the Software without
restriction, including without limitation the rights to use,
copy, modify, merge, publish, distribute, sublicense, and/or
sell copies of the Software, and to permit persons to whom the
Software is furnished to do so, subject to the following
conditions:

The above copyright notice and this permission notice shall be
included in all copies or substantial portions of the Software.

THE SOFTWARE IS PROVIDED "AS IS", WITHOUT WARRANTY OF ANY
KIND, EXPRESS OR IMPLIED, INCLUDING BUT NOT LIMITED TO THE
WARRANTIES OF MERCHANTABILITY, FITNESS FOR A PARTICULAR PURPOSE
AND NONINFRINGEMENT. IN NO EVENT SHALL THE AUTHORS OR COPYRIGHT
HOLDERS BE LIABLE FOR ANY CLAIM, DAMAGES OR OTHER LIABILITY,
WHETHER IN AN ACTION OF CONTRACT, TORT OR OTHERWISE, ARISING
FROM, OUT OF OR IN CONNECTION WITH THE SOFTWARE OR THE USE OR
OTHER DEALINGS IN THE SOFTWARE.
=============================================
*/
// Arduino Wire library is required if I2Cdev
//I2CDEV_ARDUINO_WIREimplementation
// is used in I2Cdev.h
//#include "Wire.h"

// I2Cdev and MPU6050 must be installed as libraries, or else
// the .cpp/.hfiles for both classes must be in the include
```

```
// path of your project
#include "I2Cdev.h"
#include "MPU6050.h"

// class default I2C address is 0x68
// specific I2C addresses may be passed as a parameter here
// AD0 low = 0x68 (default for InvenSense evaluation board)
// AD0 high = 0x69
//MPU6050 accelgyro;

MPU6050 accelgyroIC1(0x68);
int mpu_signal = 0;
int16_t ax, ay, az;
int16_t gx, gy, gz;

float a[3], g[3];
float pitch, roll;
float p = 0;
float r = 0;
float pitchAcc, rollAcc;
float timer = 0;
float delta_t = 0;

#define LED_PIN 13
bool blinkState = false;

void setup() {
// join I2C bus (I2Cdev library doesn't do this automatically)
Wire.begin();

// initialize serial communication
// (38400 chosen because it works as well at 8MHz as it does at
// 16MHz,but it's really up to you depending on your project)
Serial.begin(38400);

// initialize device
Serial.println("Initializing I2C devices...");
//accelgyro.initialize();
accelgyroIC1.initialize();

// verify connection
Serial.println("Testing device connections...");
Serial.println(accelgyroIC1.testConnection() ?
"MPU6050 #1 connectionsuccessful":"MPU6050 connection failed");
```

```
// configure Arduino LED for
pinMode(LED_PIN, OUTPUT);


}


void loop() {
// read raw accel/gyro measurements from device
timer = micros();
accelgyroIC1.getMotion6(&ax, &ay, &az, &gx, &gy, &gz);

// these methods (and a few others) are also available
//accelgyro.getAcceleration(&ax, &ay, &az);
//accelgyro.getRotation(&gx, &gy, &gz);


//Read Sensors Voltage levels
a[0] = ax*2.0/32768.0;
a[1] = ay*2.0/32768.0;
a[2] = az*2.0/32768.0;

g[0] = (gx * 250.0) / 32768.0 * PI/180;
g[1] = (gy * 250.0) / 32768.0 * PI/180;
g[2] = (gz * 250.0) / 32768.0 * PI/180;
/*
// display tab-separated accel/gyro x/y/z values
Serial.print("MPU:\t");
Serial.print(a[0]); Serial.print("\t");
Serial.print(a[1]); Serial.print("\t");
Serial.print(a[2]); Serial.print("\t");
Serial.print(g[0]); Serial.print("\t");
Serial.print(g[1]); Serial.print("\t");
Serial.print(g[2]); Serial.println("\t");
*/
delta_t = micros() - timer;

pitch = ComplementaryFilterY(ax, ay, az, gy, pitch);
roll = ComplementaryFilterX(ax, ay, az, gx, roll);
//Serial.print("p\t");
//Serial.print(pitch1);

Serial.print("p\t");
Serial.print(pitch);
Serial.print("\t␣r\t");
Serial.println(roll);
//Serial.println(micros() - timer);
```

```
//Output data

}

float ComplementaryFilterY(int16_t ax,int16_t ay,int16_t az,
int16_t gy, float pitch) {
long squaresum =(long)ay*ay+(long)az*az;
pitch += (-gy*250.0 / 32768.0)*(delta_t/1000000.0f);
pitchAcc = atan(ax/sqrt(squaresum))*180/PI;
pitch = 0.98*pitch + 0.02*pitchAcc;
return pitch;
}

float ComplementaryFilterX(int16_t ax,int16_t ay,int16_t az,
int16_t gx, float roll) {
long squaresum =(long)ax*ax+(long)az*az;
roll += (-gx*250.0 / 32768.0)*(delta_t/1000000.0f);
rollAcc = atan(ay/sqrt(squaresum))*180/PI;
roll = 0.98*roll + 0.02*rollAcc;
return roll;
}
```

B.2 Mathematical modeling and simulation

All required files have been included in a Github repository that can be accessed through the link:`https://github.com/namita-kumar/GymballModel/`. Note that the link corresponds to the attempted modeling of the final design. As stated earlier, the mass matrix was too close to singularity and the equations could not be solved.

To resolve the issue, the model constructed in Simscape was used to determine the torques generated by the device.
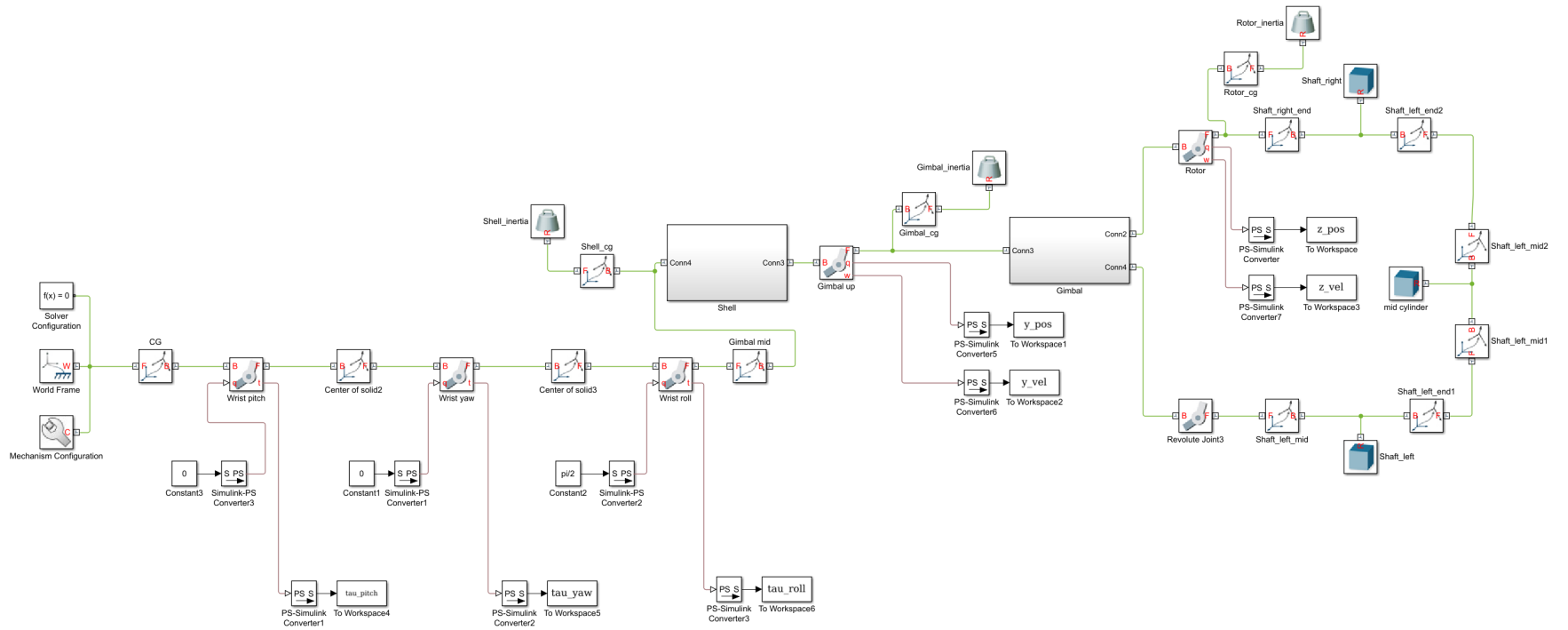
B.2.1 Simscape model

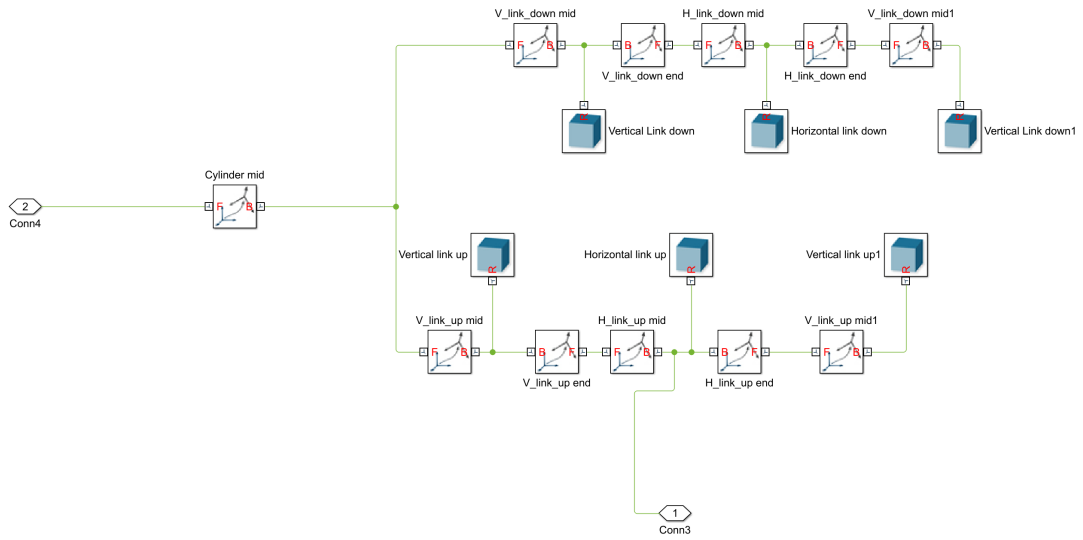Figure B.7: Simscape model of the entire gyroscopic assembly

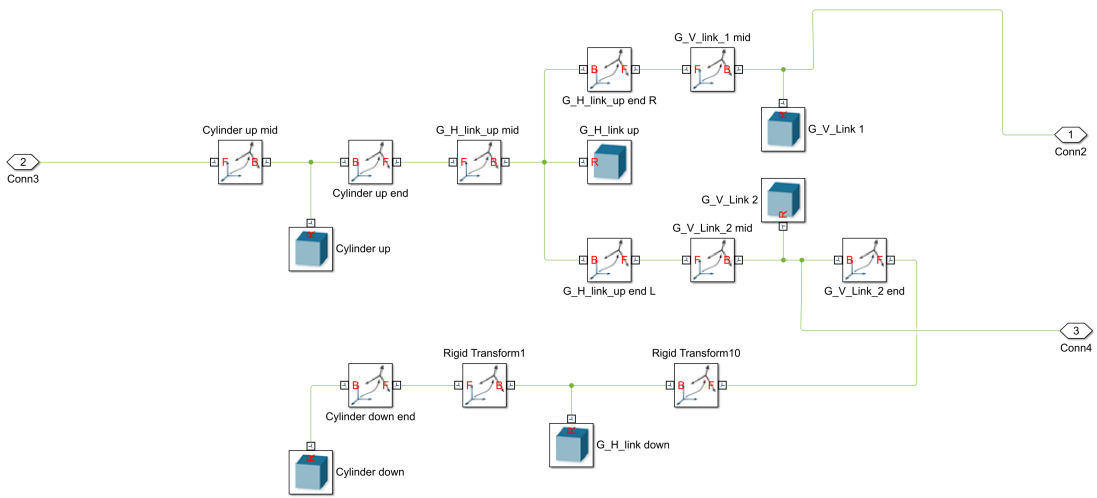Figure B.8: Simscape model of the gimbal assembly

Figure B.9: Simscape model of the rotor assembly

APPENDIX C

ANALYSIS OF FINAL DESIGN

C.1   Material properties

The following are the material properties of the print materials.

Table C.1: Material properties of Alumide [10]

Property	Value	Unit
Density	1.36	g/cm^3
Young's modulus	3600	MPa
Flexure strength	72	MPa
Tensile strength	48	MPa

Table C.2: Material properties of PA 2200 [10]

Property	Value	Unit
Density	0.93	g/cm^3
Young's modulus	1500	MPa
Flexure strength	58	MPa
Tensile strength	48	MPa

C.2 Biomechanical Analysis

The Matlab code and related data have been included in a Github repository that can be accessed through the link:

`https://github.com/namita-kumar/GymballBiomechAnalysis/.`